

The Hitchhiker’s Guide to the Outer Solar System*

Masahiro Ono[†] Marco Quadrelli[‡] Gregory Lantoine[§] Paul Backes[¶]
Alejandro Lopez Ortega^{||} Håvard Grip^{**} and Chen-Wan Yen^{††}
Jet Propulsion Laboratory, California Institute of Technology, Pasadena, CA.

David Jewitt^{‡‡}

University of California, Los Angeles, Los Angeles, CA.

We propose a novel deep space propulsion method called the *Comet Hitchhiker*. The concept is to perform momentum exchange with small bodies (i.e., asteroid and comet) using an extendable/retrievable tether and a harpoon. Unlike previously proposed tethered fly-by, the use of extendable tether enables to change the relative speed with a target. Hence Hitchhiker would be a prospective means of providing orbit insertion ΔV , particularly for rendezvous missions to small bodies in the outer Solar System such as Kuiper belt objects and Centaurs, which are not easily manageable with chemical propulsion or solar electric propulsion. Furthermore, by applying regenerative brake during a hitchhike maneuver, a Hitchhiker can harvest energy. The stored energy can be used to make a departure from the target by quickly retrieving the tether, which we call a *inverse hitchhike maneuver*. By repeating hitchhike and inverse Hitchhike maneuvers, a Hitchhiker could perform a mission to rendezvous with multiple targets efficiently, which we call a *multi-hitchhike mission*.

We derive the basic equation of Hitchhiker, namely the *Space Hitchhike Equation*, which relates the specific strength and mass fraction of tether to achievable ΔV . We then perform detailed feasibility analysis through finite element simulations of tether as well as hypervelocity impact simulations of the harpoon using the Adaptive Mesh Refinement Objected-oriented C++ (AMROC) algorithm. The analysis results suggest that a hitchhike maneuver with $\Delta V \approx 1.5 \text{ km/s}$ is feasible with flight proven materials such as Kevlar/Zylon tether and tungsten harpoon. A carbon nanotube tether, combined with diamond harpoon, would enable $\sim 10 \text{ km/s}$ hitchhike maneuver. Finally, we present two particular mission scenarios for Hitchhiker: Pluto rendezvous and a multi-hitchhike mission to the Themis family asteroids in the main belt.

I. Introduction

A. Background

One of the missing piece in Solar System exploration is rendezvous with small bodies in the outer Solar System^a, such as Kuiper Belt Objects (KBOs), Centaurs (short-lived objects interacting strongly with the giant planets), and Jupiter Trojans. Such a mission is not easily manageable with existing technologies for two reasons. First, orbit insertion around a small body requires significantly greater ΔV than around a planet because it cannot exploit the gravity of the target body. For example, the Saturn orbit insertion for Cassini required 0.62 km/s of ΔV . If Saturn were a small body, it would require $\sim 6 \text{ km/s}$. This level of maneuver would not be realistic for chemical propulsion. Second, Solar electric propulsion (SEP) is not generally effective in the outer Solar System. For these reasons all the previous rendezvous missions to small bodies have been limited to the inner Solar System.

*Copyright 2015. All rights reserved. U.S. Government Sponsorship Acknowledged.

[†]Research Technologist, Robotic Controls and Estimation Group, 4800 Oak Grove Drive, ono@jpl.nasa.gov. Member AIAA.

[‡]Group Leader, Robotic Controls and Estimation Group, 4800 Oak Grove Drive, Marco.B.Quadrelli@jpl.nasa.gov. Associate Fellow AIAA.

[§]Mission Design Engineer, Outer Planet Mission Analysis Group, 4800 Oak Grove Drive, Gregory.Lantoine@jpl.nasa.gov.

[¶]Group Supervisor, Robotic Manipulation and Sampling Group, 4800 Oak Grove Drive, paul.g.backes@jpl.nasa.gov.

^{||}Research Technologist, Electric Propulsion Group, 4800 Oak Grove Drive, Alejandro.Lopez.Ortega@jpl.nasa.gov. Member AIAA.

^{**}Research Technologist, Robotic Controls and Estimation Group, 4800 Oak Grove Drive, Havarad.F.Grip@jpl.nasa.gov.

^{††}Principal, Outer Planet Mission Analysis Group, 4800 Oak Grove Drive, Chen-Wan.L.Yen@jpl.nasa.gov. Member AIAA.

^{‡‡}Professor, Department of Earth, Planetary and Space Sciences and the Department of Physics and Astronomy, 595 Charles Young Drive East, jewitt@ucla.edu.

^a“Outer Solar System” is a loosely defined terminology. In this paper we use this term to mean the domain beyond the main asteroid belt.

Despite the unavailability of enabling technologies, small bodies in the outer Solar System are by no means negligible targets for exploration. Astronomical discoveries on distant small bodies since 1990s has provided a broad context from which the nature and evolution of the small-body populations can in principle be understood. We now understand that the Kuiper belt feeds a rain of small-bodies into the inner solar system, from the Centaurs (short-lived objects interacting strongly with the giant planets), to the Jupiter family comets (Centaurs trapped by Jupiter) to the dead remnants in the near-Earth population. Discovery and exploration of the Kuiper belt has, in particular, triggered a dramatic burst of new understanding concerning the origin and evolution of the solar system. Notably, the discovery of heavily-populated Kuiper belt mean-motion resonances requires planetary migration, which in turn implies a solar system dynamical history much more complex and less predictable than previously assumed.

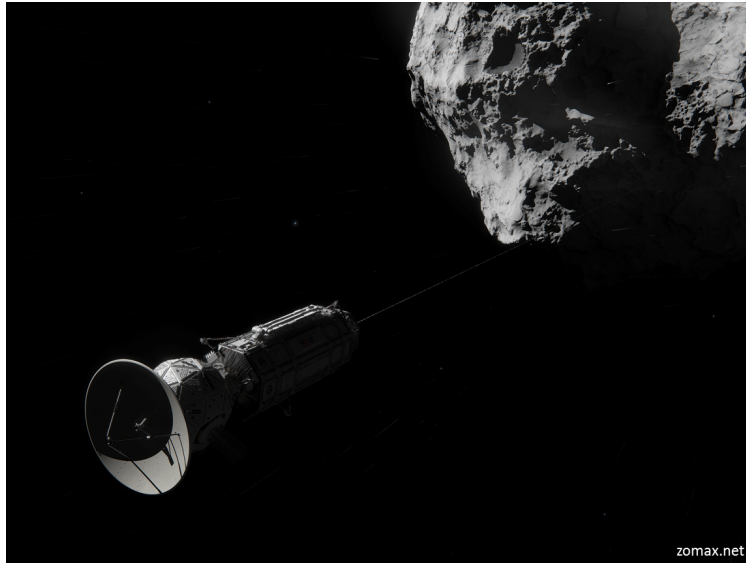


Figure 1: Concept drawing of Comet Hitchhiker.

The importance of rendezvous over fly-by missions cannot be overstated. Compare, for example, ESAs Giotto fly-by mission to comet Halley with their rendezvous mission to 67P/Churyumov-Gerasimenko. The former was able only to establish the approximate size and shape of the nucleus and provided limited compositional data from mass-spectrometers on-board. The latter is revealing the entire surface of 67P at meter-scale resolution, opening up new avenues in planetary geology, providing detailed compositional information and allowing the temporal variation of the activity to be measured as the comet sweeps through perihelion. There is even the prospect of an internal structure map from long wavelength radio penetration. In addition to providing high-resolution, multi-wavelength mapping of the entire surface of a body, invaluable for understanding its surface processes, rendezvous missions offer the possibility to determine masses and densities, to determine internal structure by gravitational anomalies and the use of long-wavelength radio waves, and to measure the time-evolution of mass loss processes from active objects. None of these quantities can be addressed from a fly-by. For these reasons, detailed investigation of small bodies in the outer Solar System through spacecraft rendezvous would be essential to ascertain the content, origin, and evolution of the Solar System. We need technologies to enable such missions.

B. Comparison with Existing/Alternative Technologies

Small body rendezvous is particularly challenging because it requires significantly greater orbit insertion ΔV than planet orbit insertion. Due to the negligible gravity of small bodies, the relative velocity between spacecraft and a target must be almost entirely killed in order to be trapped by the gravity of the target. For example, inserting New Horizons into a circular orbit around Pluto would require ~ 12.5 km/s of orbit insertion ΔV . In order to perform the orbit insertion maneuver with a chemical engine (assuming $ISP = 312$ sec, same as Cassinis main engine), 98.3% of the mass of the spacecraft must be propellant. In other words, in order to put a spacecraft with 0.5 metric tons of dry mass (approximately the same as New Horizons) around a Pluto orbit, a spacecraft with ~ 30 tons of wet mass must be injected to a trans-Pluto orbit.

Figure 2 shows approximate orbit insertion ΔV for various targets in the Solar System as well as the approximate domains covered by existing deep space propulsion methods i.e., chemical propulsion and SEP^b. Although chemical propulsion can be used at any distance from Sun, the realistic level of orbit insertion ΔV that it can provide is a few km/s at most. While Solar electric propulsion (SEP) can provide significantly greater ΔV , it is not a realistic option in the outer Solar System due to insufficient Solar flux. An alternative deep space propulsion method is solar sail, which has been flight validated by the IKAROS mission.²⁰ However, like SEP, solar sail can provide ΔV only in the inner Solar System.

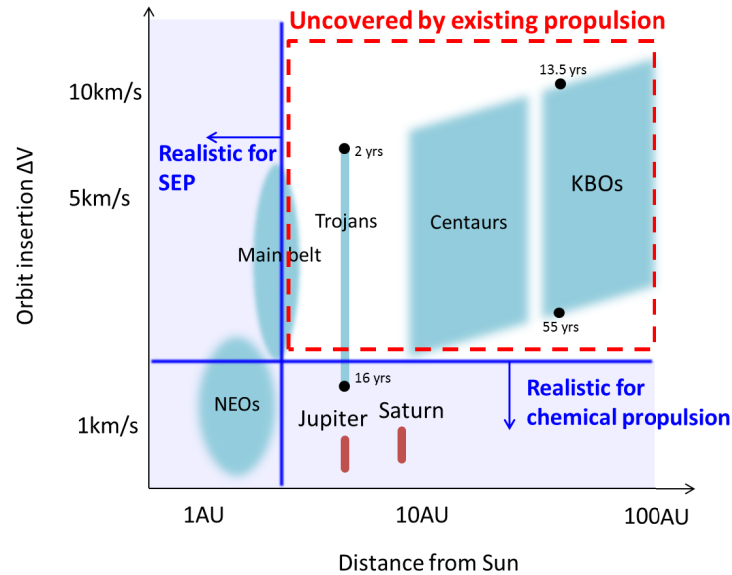


Figure 2: Orbit insertion ΔV for various targets in the Solar System and the approximate domains covered by existing deep space propulsion methods (chemical propulsion and SEP). Chemical propulsion can be used at any distance from Sun but the achievable ΔV is limited. SEP can achieve significantly A higher ΔV but its use is limited in the inner Solar System. A hitchhiker has potential to push these boundaries.

Potential future propulsion methods for outer Solar System exploration include radioisotope electric propulsion (REP)¹² and nuclear thermal propulsion. REP combines a radioisotope thermoelectric generator (RTG) with ion thrusters. While it is suitable for long-duration mission in the outer Solar System, its low specific power (i.e., power-to-weight ratio) is a challenge. In order to provide reasonable mission times and performance for rendezvous missions in the outer Solar System, specific power of 7 to 10 We/kg are needed, which in turn requires light-weight, high-performance RTGs and ion thrusters.¹² The GPHS RTG, which was used for Galileo, Cassini, and New Horizons missions but is no longer in production, has a specific power of ~ 5 We/kg at the beginning of life;¹¹ the MMRTG, which is the current option for future NASA missions, has a specific power of 2.8 We/kg. Since the efficiency of state-of-the-art ion-thrusters is $\sim 60\%$, the combined specific power of REP would be ~ 3 We/kg with GPHS RTG and ~ 1.7 We/kg with MMRTG. Stirling radioisotope power, which converts radioisotope heat to electricity using a piston-powered generator, could provide higher specific power (e.g., the canceled ASRG would have provided 3.5 - 7 We/kg⁵) but still insufficient for outer Solar System rendezvous missions. Supply shortage of plutonium-238 is another issue, although it is being addressed by current NASA funding for the Department of Energy to produce more Pu-238 in the 2020's. Nuclear thermal propulsion could provide an ultimate solution, but its cost, complexity, and safety are major issues.

An alternative is a non-propulsive approach. Since orbit insertion is essentially to kill the relative velocity between the spacecraft and the target body, it can be done by applying “brake”, or exchanging momentum with the target. For example, aerocapture, aerobraking, and direct atmospheric entry can be viewed as momentum exchange through atmosphere. In fact, Mars surface exploration is significantly assisted by the fact that a lander can save ~ 7 km of ΔV

^bNote that, as we analyze in detail in Section VI, there are diverse options of trajectory to get to a target. In general, a trajectory with a lower orbit insertion ΔV requires a longer flight time. For example, in case of Pluto, a trajectory with 13.5 year transfer time requires 10 km of orbit insertion ΔV , while one with 55 year transfer time requires 2.5 km/s of ΔV . (See Section VI-B for details.)

for nulling the relative velocity by direct atmospheric entry. When the target lacks a medium for momentum exchange such as atmosphere, spacecraft can bring the medium, which is specifically a tether. The basic idea of the Hitchhiker is to harpoon a target to attach a tether, and use the tether to exchange the momentum and “stop” the spacecraft in relative to the target. We call such a maneuver a *space hitchhike maneuver*, which is illustrated in Figure 3 and explained in detail Section II-A. Furthermore, a hitchhiker spacecraft that is already in the orbit or on the surface of a small body can make a departure (i.e., gaining relative speed) by inverting the hitchhike process. We call such a maneuver an *inverse space hitchhike maneuver*, which is illustrated in Figure 4 and explained in detail Section II-B.

Our concept brings important advantages over a related concept of tether-based fly-by,¹⁶ which uses a fixed length of tether in order to change the direction of the relative velocity like a gravity assist. This concept cannot be used for landing and orbit insertion because it does not reduce the relative speed. The comet hitchhiker concept is distinct in that it reels out a tether while applying regenerative brake force to accelerate itself. This approach allows the spacecraft to match its velocity with that of the target, and as a result, enables soft landings and orbit insertion.

The rest of this paper is organized as follows. First, Section II introduces the concept of Hitchhiker. Section III derives the Space Hitchhike Equation and presents the results of the finite element simulation of tether dynamics to evaluate feasibility. Section IV then presents the result of hypervelocity impact simulation of harpoon to assess the feasibility of harpoon-based tether attachment to a small body. Section V introduces the brake mechanisms that could be used for Hitchhiker. Finally, Section VI presents two sample missions scenarios, a rendezvous mission to Pluto and a multi-rendezvous mission in the main asteroid belt.

II. Concept

The Comet Hitchhiker concept is essentially to perform momentum exchange with a target body using an extendable/retrievable tether. The momentum exchange is performed in two ways: i) to kill the relative velocity with the target, and ii) to accelerate the spacecraft in relative to the target. We call the former a *space hitchhike maneuver*, while the latter is called an *inverse space hitchhike maneuver*. The most unique aspect of the concept is to use extendable/retrievable tether, which enables: 1) to control the spacecraft acceleration within a tolerable level, 2) to absorb jerks, 3) to harvest the kinetic energy of the target body, and most importantly, 4) to change or completely kill the relative velocity with the target, hence enabling rendezvous and landing.

A. Space Hitchhike Maneuver

As illustrated in Figure 3, first, the spacecraft would harpoon a target as it makes a close fly-by in order to attach a tether to the target. Then, as the target moves away, it would reel out the tether while applying regenerative braking to give itself a moderate ($<5g$) acceleration. If there is a sufficient length of tether, the spacecraft can eventually make the relative velocity sufficiently small so that it is captured by the weak gravity of the target. At the end of the hitchhike maneuver, the spacecraft would be at a significant distance from the target - typically 10-1000 km, depending on the initial relative velocity. Closing in on the target is easy because the relative velocity has already been killed. The spacecraft can simply retrieve the tether slowly to come closer to the target, and possibly land on it.

This idea can be intuitively understood by the analogy of fishing. Imagine a fisherman on a small boat trying to catch a big fish that swims at a high relative speed. Once the fish is on a hook, the experienced fisherman would let the line go while applying a moderate tension on it, instead of holding it tightly. If the line has a sufficient length, the boat can eventually catch up with the fish with moderate acceleration.

In addition, by applying regenerative braking, a Comet Hitchhiker could harvest energy from the target body. Assuming 25% efficiency of a regenerative brake, a 2-ton comet hitchhiker can produce ~ 25 GJ of energy, which is sufficient to drive an instrument with 1 kW power consumption over 290 days. If future storage devices can achieve the energy density of gasoline, 25 GJ can be stored in 500 kg of mass, making it a potential energy source in the outer Solar System.

B. Inverse Space Hitchhike Maneuver

In order to rendezvous with multiple targets in a single mission, a hitchhiker also needs to be able to depart from a target. A hitchhiker would make a fuel-less acceleration by performing an inverse hitchhiker maneuver, as shown in Figure 4. First, when the hitchhiker is on the surface or in orbit, it would attach a tether to the target. Next, it would slowly move away from the target while deploying the tether. Then, it would accelerate itself by pulling in the tether. The energy harvested from the previous hitchhike maneuver could be used to pull in the tether. Finally, once the desired velocity is achieved, the spacecraft would detach the harpoon and fly away to the next target.

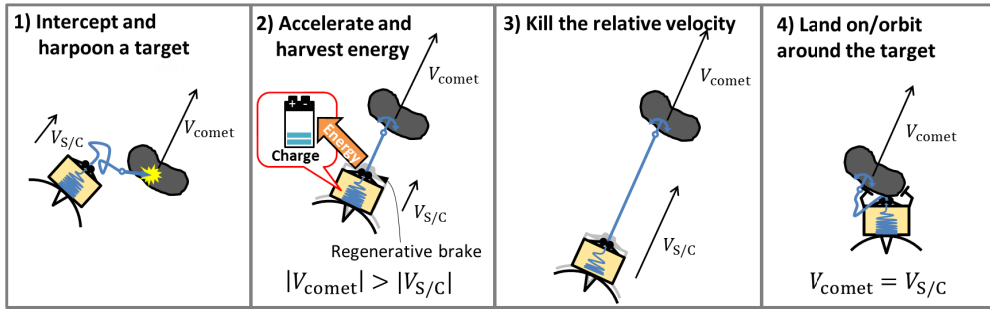


Figure 3: Space hitchhike maneuver for small body rendezvous/landing

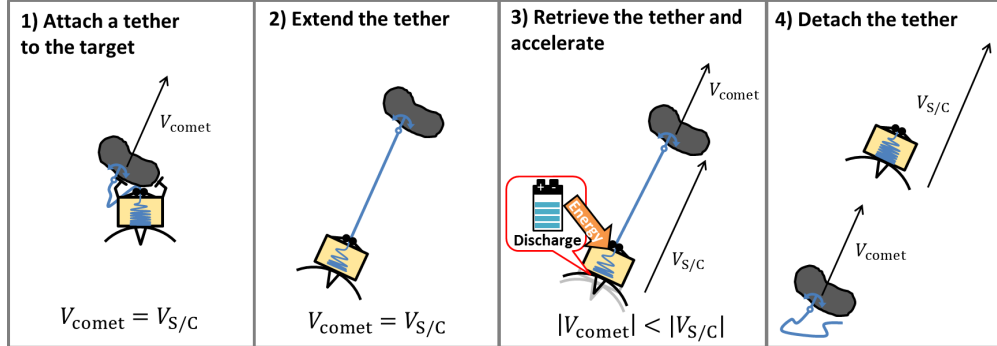


Figure 4: Inverse hitchhike maneuver to depart from a small body

C. Sample Mission Concept

Figure 5 shows a sample scenario of a hitchhiker mission. A hitchhiker would be launched to an interplanetary trajectory by a conventional rocket. Fly-by missions such as *Voyager* and *New Horizon* used gravity assist in order to increase orbital speed. Gravity assist is a useful tool for a hitchhiker mission but for a different purpose: to raise the perihelion and decrease the orbit insertion ΔV (hence the orbital speed is typically decreased). Upon the arrival at a small body in the outer Solar System, the hitchhiker would perform a space hitchhike maneuver and rendezvous with the target. After completing the investigation, it would depart from the target by performing an inverse space hitchhike maneuver and go to the next target. By repeating multiple hitchhike and inverse hitchhike maneuvers, the hitchhiker can visit multiple targets in a single mission. A similar multi-rendezvous tour could also be performed in the Kuiper belt and the main belt. Optionally, the launch C_3 could be reduced by accelerating with hitchhike maneuvers at near Earth objects (NEOs) and short-period comets. Concrete mission scenarios and trajectory analyses are presented in Section VI.

III. Hitchhiker Dynamics and Performance

In this section, we first derive the basic equation of the Hitchhiker concept, namely the *Space Hitchhike Equation (SHE)*. Like the Tsiolkovsky rocket equation relates the specific impulse and the propellant mass fraction to ΔV , SHE relates the specific strength and mass fraction of tether to ΔV . We then perform finite-element simulation in order to validate SHE as well as to analyze the basic feasibility of the Hitchhiker concept.

A. Space Hitchhike Equation (SHE)

1. Overview

In this section we consider the space hitchhike maneuver. The same derivation process applies to the inverse space hitchhiker maneuver by flipping signs.

The tension of the tether must be controlled to be within the tensile strength. The tension of the tether plays two

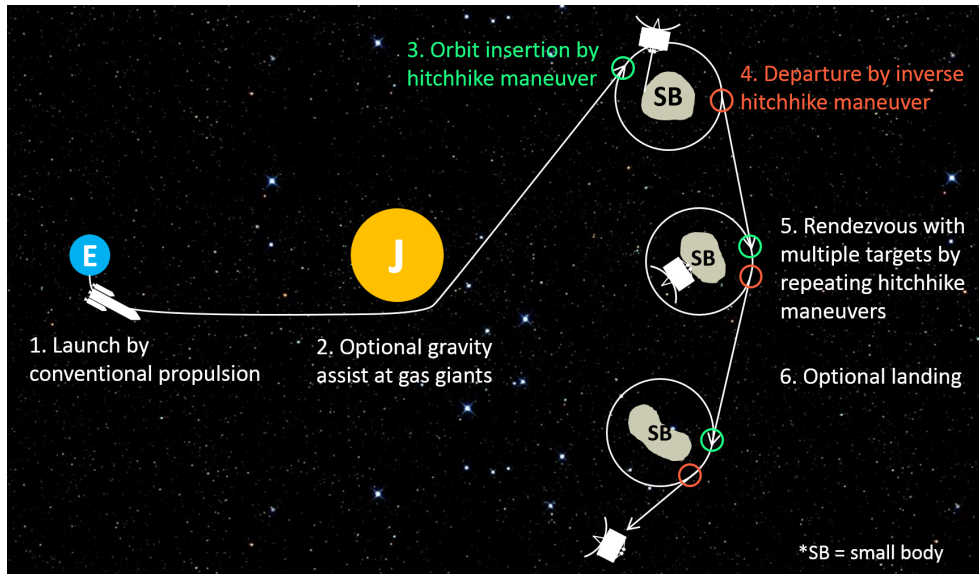


Figure 5: Sample mission scenario with a hitchhiker rendezvousing with multiple small bodies in the outer Solar System.

roles: accelerating S/C, and accelerating the tether itself. Hence,

$$(\text{Total tension}) = (\text{Tension to accelerate S/C}) + (\text{Tension to deploy tether}).$$

As for the left hand side, the maximum total tension that a tether can tolerate is constant. As for the second term of the right hand side, the tension required to deploy the tether is given by $\frac{dm}{dt}v$, where $m(t)$ is the mass of tether that has not been deployed at t (i.e., the mass of tether in the spacecraft) and v is the velocity of tether deployment. Intuitively, $\frac{dm}{dt}$ represents the mass of the tether that needs to be accelerated for a unit time period, and v represents the magnitude of the velocity change of the tether. In our case, the tension that is used to accelerate the tether decrease over time, since both $\frac{dm}{dt}$ and v decreases over time. Therefore, the tension that can be used for accelerating the spacecraft increases over time. As a result, in order to maximize the ΔV with a given tensile strength of a tether, a hitchhiker should increase the acceleration over time. Thus, to achieve the maximum, the S/C must be equipped with a tether control device (i.e., brake) that can control the tension. Existing brake mechanisms, such as linear Eddie current brake, can control the brake force, as explained in Section V.

In the following subsections, we first derive SHE. We then use the equation to estimate the achievable ΔV with different tether materials.

2. Derivation of the Space Hitchhike Equation

As shown in Figure 7, we assume a hitchhike maneuver where the spacecraft travels at a relative velocity V at the beginning, and completely kills the relative velocity at the end of the maneuver. Let v and m be the relative velocity and the mass of spacecraft. The latter include the mass of undeployed tether. Hence, both v and m decreases over time since the S/C decelerates as deploying the tether. Let σ , ρ , and A be the tensile strength, density, and the section area of the tether, which are assumed to be uniform. The tethers tension is maximum at the attachment to the target body. We denote this tension by T .

As we discussed, the tension of the tether is the sum of the tension required to accelerate the S/C and the tension required to accelerate the tether. Therefore,

$$-\frac{dv}{dt}m - \frac{dm}{dt}v = T. \quad (1)$$

The spacecraft deploys the tether at the speed of v . Therefore, the rate of change of the S/Cs mass is given by:

$$\frac{dm}{dt} = -A\rho v. \quad (2)$$

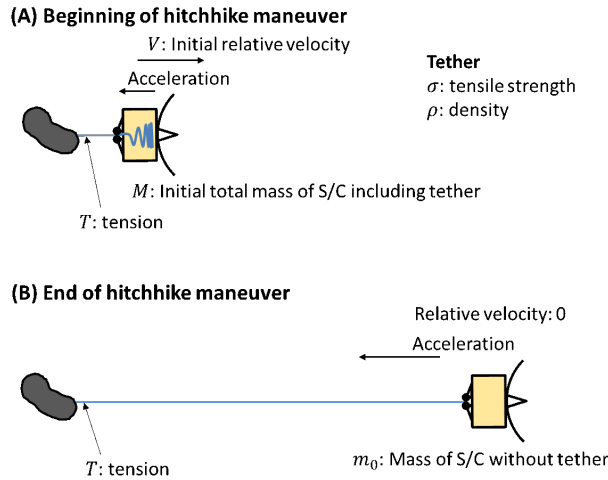


Figure 6: Assumptions used in the derivation of the Space Hitchhike Equation

The upper bound of the tolerable tension is given by the tensile strength of the material of the tether:

$$T = A\sigma. \quad (3)$$

By substituting (2) and (3) to (1), we get

$$\frac{dv}{dt} = -\frac{A}{m}(\sigma - \rho v^2). \quad (4)$$

Eliminate t by dividing (4) by (2):

$$\frac{dv}{dm} = \frac{1}{\rho m v}(\sigma - \rho v^2) \quad (5)$$

This ordinary differential equation is separable as follows:

$$\frac{2v}{(\sigma/\rho) - v^2} dv = 2 \frac{dm}{m}. \quad (6)$$

This can be solved as follows:

$$-\log\left(\frac{\sigma}{\rho} - v^2\right) = \log m^2 + C, \quad (7)$$

where C is a constant. By substituting the terminal conditions, $v_0 = 0$ and $m = m_0$, we obtain:

$$C = -\log m_0^2 - \log\left(\frac{\sigma}{\rho}\right). \quad (8)$$

Finally, by eliminating C in the general solution (7) by (8), we obtain the following:

$$1 - \frac{\rho}{\sigma} v^2 = \left(\frac{m_0}{m}\right)^2. \quad (9)$$

By solving (9) for v and replace m with M , the initial total mass of spacecraft, we obtain the following Space Hitchhike Equation that gives the upper bound on the ΔV :

$$\Delta V = \sqrt{\frac{\sigma}{\rho} \left\{ 1 - \left(\frac{m_0}{M}\right)^2 \right\}} \quad (10)$$

In the above equation, σ/ρ (tensile strength divided by density) is called the *specific strength* of a material. m_0/M is the ratio between the spacecraft mass before and after the hitchhike maneuver, which is simply called the *mass ratio*. SHE relates specific strength, mass ratio, and ΔV , just like the Tsiolkovsky rocket equation relates specific impulse, mass ratio, and ΔV .

3. Interpretation of the Space Hitchhike Equation

While hitchhike maneuver does not require propellant, it requires tether, which occupies a certain portion of the total mass of the S/C. The more tether the S/C has, the more ΔV it can achieve. Therefore, the tether of a hitchhiker is analogous to the propellant of a chemical rocket, except that it can be used multiple times.

Figure 7 plots the mass ratio, M/m_0 , against ΔV for hitchhikers with different tether materials as well as for a conventional propulsion with 300 sec ISP. Intuitively, M/m_0 is the “wet mass” of the spacecraft (i.e., mass including tether or propellant) that is required to provide a given ΔV to a unit mass of payload.

The shape of the curve is very different between hitchhike and conventional propulsion. As is well known, for conventional propulsion, the mass ratio grows exponentially with ΔV . In theory, it can achieve any ΔV . However, in practice, the exponential growth in the mass ratio makes it impractical to perform a large ΔV maneuver. On the other hand, the curve of a hitchhiker has a mirrored “L shape. There is an absolute upper bound on ΔV , meaning that no matter how large the mass ratio is, there is an upper limit on ΔV that cannot be exceeded. The limit is shown in the vertical dashed lines in Figure 7. However, the growth of the mass ratio is slow except for the proximity of the upper bound.

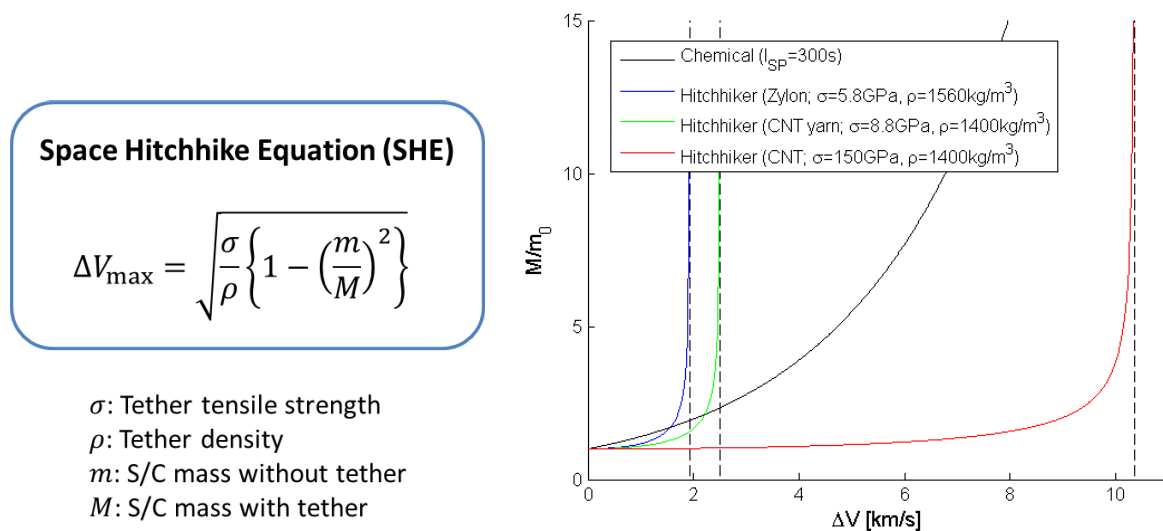


Figure 7: Left: Space Hitchhike Equation. Right: Required mass ratio to achieve a given ΔV .

B. Hitchhiker Performance for Specific Tether Materials

SHE tells that, in order to achieve greater ΔV , we need a tether material that has higher specific strength. Intuitively, a tether should be stronger and lighter.

1. Flight-Proven Materials: Zylon and Kevlar

Among flight proven materials, Zylon has the strongest specific strength. For example, in the Mars Exploration Rovers mission, a nearly 20-meter-long (65-foot-long) braided Zylon was used as a bridle connecting a parachute and the lander. The blue curve in Figure 7 shows the SHE curve of Zylon. Its upper bound on ΔV is 1.93 km/s. Although it outperforms chemical propulsion when ΔV is less than 1.56 km/s, the advantage is marginal. However, the advantage would become nontrivial when it is used for a multi-hitchhike mission.

Kevlar is also a flight proven material with a very high specific strength, but slightly lower than Zylon.

2. Carbon Nanotubes

Carbon nanotubes (CNTs) have the largest specific strength among known materials; it was reported that ~ 150 GPa tensile strength has achieved.³ This level of tensile strength enables a radical hitchhike maneuver. The red line in Figure 7 is the SHE curve of a CNT fiber. The upper bound on ΔV is 10.4 km/s. It significantly outperforms chemical

propulsion for most of the domain below the bound. Importantly, this domain covers the orbit insertion ΔV for the rendezvous missions to KBOs, (~ 10 km/s), Centaurs (7.3 km/s), and Jovian Trojans (7 km/s), as discussed in Section VI. For example, in order to give 7.3 km/s ΔV , the mass ratio required for a hitchhiker is only 1.41, while chemical propulsion requires 12.0.

A present issue of CNTs is that only short fibers are available. Although manufacturing a long CNT fiber is an active area of research, the longest fiber to date is ~ 50 cm,²² which is clearly insufficient for hitchhikers.

3. Carbon Nanotube Yarns

Production technology of CNT yarn, a tether made of multitudes of short CNT fibers, is also a very active topic of research. It was reported that up to 1 km long CNT yarn has been available.¹⁵ To date, the best tensile strength that has been achieved is 8.8 GPa,¹ which has already exceeded Kevlar and Zylon but still far from the strength of CNT fibers.

The green line in Figure 7 is the SHE curve for CNT yarn. Up to 2.51 km/s ΔV is achievable with a hitchhiker with a currently available CNT yarn.

In summary, the utility of the Comet Hitchhiker concept rests upon future development in material. Realizing 100 GPa-level tensile strength would open the door for various exciting science missions by using hitchhikers. Alternatively, by repeating 1-2 km/s hitchhike maneuvers with existing material like Zylon could also give hitchhiker a significant advantage over existing propulsion methods.

C. Tether Deployment

Two concerns when deploying a tether at a high velocity are tension and stability. It turns out that SHE is a sufficient condition for deployment speed in terms of both tension and stability, as discussed below.

TENSION The required tension to pull out a tether at velocity v is ρAv^2 , where A is the section area of tether. This tension is included in the derivation of SHE. Therefore, when the initial relative velocity is within the bound given by SHE, the tension does not exceed the tensile strength of tether.

STABILITY It is known that if a tether is deployed at a speed greater than the speed of sound on the tether (i.e., the transverse wave velocity) the tether dynamics is unstabilized, meaning that the deflection is amplified as tether is deployed.⁸ The speed of sound on tether is $\sqrt{T/A\rho}$, where T is the tension. Since the tension is bounded by σA , the speed of tether deployment must be less than $\sqrt{\sigma/\rho}$. Note that this bound is always greater than the bound given by SHE. Therefore, SHE is a sufficient condition for tether deployment stability.

D. Finite-element Simulation

1. Modeling Approach

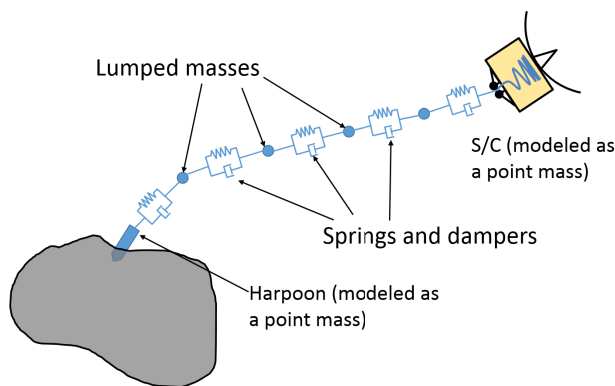


Figure 8: Finite-element model of tether used for simulations

We modeled a tether by a finite number of lumped mass, connected by a chain of springs and dampers, as shown in Figure 8. The entire system is modeled in 2D by representing the spacecraft and harpoon as two point masses with

the following nominal equations of motion:

$$\dot{p}_s = v_s, \quad (11a)$$

$$m_s \dot{v}_s = F_s, \quad (11b)$$

$$\dot{p}_h = v_h, \quad (11c)$$

$$m_h \dot{v}_h = F_h, \quad (11d)$$

where p_s and p_h are the respective positions of the spacecraft and harpoon; v_s and v_h are the respective velocities; m_s and m_h are the respective masses (with any undeployed tether included in m_s); and F_s and F_h are the respective forces acting on the bodies. The comet is assumed to be massive compared to the spacecraft and the harpoon, and it is therefore modeled as a stationary ellipsoidal body.

At the start of each simulation, the spacecraft is initialized some distance away from the comet with a non-zero relative velocity. The harpoon is initially co-located with the spacecraft, but diverges at a rate corresponding to the harpoon ejection velocity. Once contact is made between the harpoon and the comet, the harpoon remains fixed (anchored) for the remainder of the simulation, and the equations of motion are simply

$$\dot{p}_h = 0, \quad (12a)$$

$$m_h \dot{v}_h = 0. \quad (12b)$$

TETHER MODELING The forces F_s and F_h in (11) arise solely due to tether interaction between the spacecraft and the harpoon. We model the tether itself by a sequence of n point masses connected to each other, as well as to the spacecraft and the harpoon, by linear spring-dampers. For each tether point mass $i \in 1, \dots, n$, ordered in the direction from the spacecraft to the harpoon, we denote by p_i and v_i the position and velocity of the tether point mass. For notational convenience, we also define $p_0 := p_s$, $v_0 := v_s$, $p_{n+1} := p_h$, and $v_{n+1} := v_h$. We label each tether segment with the index of the inboard body to which it connects; for example, segment 0 is the segment connected to the spacecraft.

Each tether point mass $i \in 1, \dots, n$, is governed by the following equation of motion:

$$\dot{p}_i = v_i, \quad (13a)$$

$$m_p \dot{v}_i = F_i - F_{i-1}, \quad (13b)$$

where m_p is the mass and F_i is the force exerted on tether point mass i by tether segment i . Accordingly, we can write $F_s = F_0$ and $F_h = -F_n$.

Tether Segments Each tether segment represents a certain length of deployed tether, characterized by a *nominal* or *unsprung* length ℓ_{0i} . The forces produced by the segment are a function of the *strain* and *strain rate* associated with the segment. The strain of segment i is defined as

$$s_i := \frac{\ell_i - \ell_{0i}}{\ell_{0i}}, \quad (14)$$

where $\ell_i = \|p_{i+1} - p_i\|$ is the current length of the tether segment. The strain rate \dot{s}_i is the rate of change in s_i .

The nominal lengths of all tether segments should add up to the total amount of currently deployed tether, which we denote by d_0 . In the course of the hitchhiking maneuver, d_0 will increase (as described in detail later on), and to account for this, we also increase the number of tether mass points. In particular, tether segments $1, \dots, n$ have a fixed nominal length denoted by $\bar{\ell}_0$, whereas segment 0 has a nominal length of $\ell_{00} = d_0 - n\bar{\ell}_0 \geq 0$, so that the sum of all nominal lengths is equal to d_0 . Once $\ell_{00} > \bar{\ell}_0$, a new tether point mass is added by splitting segment 0. The position of the new point mass is chosen so that the strain in each new spring segment is equal to that of the original segment, which for practical purposes places it very close to the spacecraft. The velocity of the new point mass is equal to that of the spacecraft.

The mass of each tether point mass corresponds to the mass of a segment of length $\bar{\ell}_0$; that is $m_i = \rho A \bar{\ell}_0$, where ρ is the tether material density and A is the section area.

Tether Forces and Deployment For each tether segment $i \in 1, \dots, n$, the force F_i is generated by a linear spring-damper model:

$$F_i = e_i T_i, \quad (15a)$$

$$T_i = K s_i + C \dot{s}_i, \quad (15b)$$

where K is a spring constant; C is a damping constant; and $e_i = (p_{i+1} - p_i)/\|p_{i+1} - p_i\|$ is the unit vector pointing from p_i to p_{i+1} .

Tether segment 0 is treated separately because it is connected to the spacecraft, where tension is actively controlled by deploying tether throughout the hitchhiking maneuver. We assume that the tension is controlled in a manner analogous to a fishing reel, which saturates at a certain level of tension. In particular, the amount of deployed tether is held constant as long as the tension felt by the spacecraft is below a certain target tension; above this level, tether is deployed in order to maintain the target level of tension. Accordingly, we model the force and rate of deployment as follows

$$F_0 = e_0 T_0, \quad (16a)$$

$$T_0 = \begin{cases} Ks_0 + C\dot{s}_0, & |Ks_0 + C\dot{s}_0| \leq T_t, \\ T_t, & \text{otherwise,} \end{cases} \quad (16b)$$

$$\dot{d}_0 = \begin{cases} 0, & |Ks_0 + C\dot{s}_0| \leq T_t, \\ e_0^T (v_1 - v_0), & \text{otherwise.} \end{cases} \quad (16c)$$

where $e_0 = (p_1 - p_0)/\|p_1 - p_0\|$. In words, the segment acts as a fixed-length spring-damper until the tension reaches a certain target level, at which point the tension is maintained at the target level and the rate of tether deployment is equal to the rate at which tether mass point 1 is moving away from the spacecraft.

Target Tension The target tension T_t depends on the phase of the hitchhiking maneuver. During the pre-anchoring phase, before the harpoon has made contact with the comet, $T_t = 0$; that is, the tether is reeled out with no resistance.

During the post-anchoring phase, the aim is to maximize the tension felt by the spacecraft without the total tension anywhere along the line exceeding some limit T_{\max} less than the tensile strength of the material. As discussed in Section III-A.1, the total tension in the tether material is a combination of the tension felt by the spacecraft and the tension needed to accelerate the tether. Only the former can be directly measured and controlled; hence an estimate of the latter must be formed in order to synthesize an appropriate target tension T_t .

Assuming for the moment that the motion is one-dimensional, we obtain the following requirement from the derivation of SHE:

$$-m_s \dot{v}_s - \dot{m}_s v_s \leq T_{\max}. \quad (17)$$

When tension is at the target level, $-m_s \dot{v}_s = T_t$, and hence we obtain the bound $T_t \leq T_{\max} + \dot{m}_s v_s$. Also from the derivation of SHE, the rate of change in mass is bounded by $\dot{m}_s \geq -\rho A v_s$, which results in the bound $T_t \leq T_{\max} - \rho A v_s^2$.

We extend this bound to the two-dimensional case in a way that is conservative but reduces to the one-dimensional bound for any one-dimensional motion:

$$T_t \leq T_{\max} - \rho A \|v_s\|^2. \quad (18)$$

SPRING AND DAMPING CONSTANTS For a given tether material, the spring constant K , which represents the tether tension due to unit strain, can be computed as $K = A\sigma_y$, where A is the sectional area and σ_y is Young's modulus. The damping constant C is less readily available; in the simulations to be presented below, we have chosen the damping arbitrarily, but we have investigated the sensitivity of the results to changes in damping.

With respect to the spacecraft velocity profile and the amount of deployed tether, the sensitivity to tether damping appears minimal even when varied by several orders of magnitude. The main observable sensitivity is in the tether dynamics, with ripples settling out slower with decreased damping. This, in turn, results in larger peak tensions along the tether line.

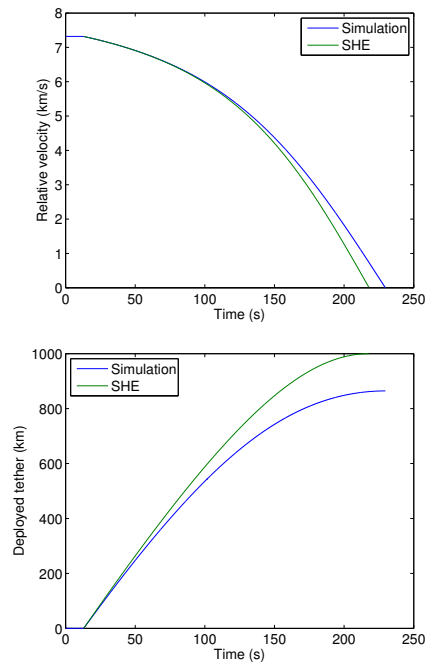
2. Comparison with SHE

The model described above can be exercised for idealized one-dimensional maneuvers and compared to SHE. As an example, consider the case outlined in Table 9a, where the spacecraft moves along a straight line and intersects the target body at a relative speed corresponding to the maximum ΔV predicted by SHE. The simulation is run with a maximum tension T_{\max} corresponding to a tensile strength of 100 GPa. The distance \bar{l}_0 between tether point masses is set to a large number in order to avoid line dynamics (i.e., the tether consists only of a single segment).

At first glance, we expect this idealized scenario to produce a deceleration to zero relative velocity while using precisely the 1000 km of available tether. In the simulation, however, only 864 km of tether is deployed; in other

	Value	Unit
Target		
Center	[0; -30]	km
Semi-axes	[60; 30.1]	km
Spacecraft		
Dry mass	1,000	kg
Initial position	[-100; 0]	km
Initial velocity	[7.32; 0]	km/s
Harpoon		
Mass	10	kg
Ejection velocity	[0; 0]	km/s
Tether		
Young's modulus	500	GPa
Density	1400	kg/m ³
Section area	$7.14 \cdot 10^{-7}$	m ²
Available length	1000	km
Damping constant	0	kNs
Maximum tension (T_{\max})	71.40	kN
Simulation		
Step size	0.01	s

(a) Simulation parameters, straight-line maneuver



(b) Profiles of relative velocity and deployed tether length

Figure 9: Parameter settings and simulation results with a straight-line maneuver. The plots compare the results of a simulated straight-line maneuver with those arising from the assumptions made in the derivation of SHE. The left figure shows the relative velocity profile and the right figure shows the amount of deployed tether as a function of time. Owing to the extensibility of the simulated tether, less tether is needed to halt the relative velocity than what is predicted by SHE.

words, a greater ΔV could have been achieved by using the entire tether. A comparison between SHE and the simulation results, in terms of relative velocity and deployed tether, can be seen in Figure 9.

The explanation for this discrepancy lies in the assumption, used in the derivation of SHE, that the rate of tether deployment is equal to the relative velocity of the spacecraft with respect to the comet (reflected in expression for the rate of mass loss). However, this is only true for a tether that is perfectly stiff; an extensible tether must be deployed at the lower rate needed to maintain approximately constant strain.^c Consequently, SHE can only be considered an upper bound on ΔV in the limiting case of an inextensible tether. Indeed, as the tether stiffness is increased in the simulation, the result converges to that predicted by SHE.

To appreciate the benefit of tether extensibility, it is informative to consider another limiting case, namely, when the tether is infinitely extensible (i.e., an ideal spring). Assuming for the sake of simplicity that the nominal length is zero, the system can be viewed as a double integrator controlled by a linear control law specifying the tension through the spring and damping constants. It is known that any linear system with no poles in the open right-half complex plane is stabilizable by an arbitrarily bounded input; moreover, for any arbitrarily large region of attraction and any arbitrary limit on the input, a stabilizing linear control law can be designed so as not to exceed the limit on the input.⁹ The cost of such a *low-gain* design is a large transient excursion called *slow peaking*. It follows from this consideration that, if the tether is arbitrarily extensible, then by decreasing the Young's modulus, one can achieve an arbitrarily large ΔV irrespective of the tether's tensile strength.

3. Simulation Results

Simulations were run for a number of different scenarios. In all cases, following harpoon touchdown, ripples can be seen developing along the tether line, the magnitude and settling dynamics depending on the damping parameter. As predicted by the theory, the rate of deceleration is initially slow, while the rate of tether deployment is high; toward the end of the maneuver, this relationship is inverted.

Compared to the one-dimensional case, a penalty is incurred because tether is deployed prior to harpoon touchdown, and because the tether force initially acts almost perpendicular to the relative velocity, only weakly opposing the relative motion. The perpendicular component of the tether force gives rise to a velocity in the same direction, resulting in a curved trajectory and a non-zero terminal velocity.

Table 1: Simulation Parameters

(a) Simulation parameters, Zylon case			(b) Simulation parameters, CNT case		
	Value	Unit		Value	Unit
Target			Target		
Center	[0; -30]	km	Center	[0; -30]	km
Semi-axes	[60; 30.1]	km	Semi-axes	[60; 30.1]	km
Spacecraft			Spacecraft		
Dry mass	1,000	kg	Dry mass	1,000	kg
Initial position	[-100; 10]	km	Initial position	[-100; 10]	km
Initial velocity	[1.67; 0]	km/s	Initial velocity	[1.67; 0]	km/s
Harpoon			Harpoon		
Mass	10	kg	Mass	10	kg
Ejection velocity	[0; -2.17]	km/s	Ejection velocity	[0; -2.17]	km/s
Tether			Tether		
Young's modulus	270	GPa	Young's modulus	270	GPa
Density	1560	kg/m ³	Density	1560	kg/m ³
Section area	$5.34 \cdot 10^{-6}$	m ²	Section area	$5.34 \cdot 10^{-6}$	m ²
Available length	120	km	Available length	120	km
Damping constant	1,000	kNs	Damping constant	1,000	kNs
Maximum tension (T_{\max})	30.97	kN	Maximum tension (T_{\max})	30.97	kN
Simulation			Simulation		
Step size	0.01	s	Step size	0.01	s
Distance between tether point masses	2	km	Distance between tether point masses	2	km

^cAccording to (16c), the rate of deployment in the simulation is equal to the rate at which the spacecraft is moving away from tether point mass number 1; when the line consists of a single segment, this is equivalent to deploying at a rate equal to the relative velocity of the spacecraft with respect to the comet. However, as soon as the tether becomes too long to produce a tension larger than T_t , the deployment stops and the tension builds back up. As a result, the tension chatters in a very narrow band around T_t and produces the correct rate of deployment over time.

Two parameterizations are shown in Tables 1a and 1b, one in which a 120 km long Zylon tether is used, and another in which a 1,000 km long CNT tether is used. Results from the Zylon case can be seen in Figure 10. In Figures 10a and 10b, the relative velocity and the amount of deployed tether is compared to SHE. It is seen that, due to the 2D penalty discussed above, more tether than the available 120 km is used; hence, in this case one would have to aim for a smaller ΔV . In Figure 10c the trajectory of the spacecraft is shown, which clearly curves in the direction of the comet (not shown).

Figure 10d indicates the maximum tension at any element along the tether, which should never exceed $T_{\max} = 30.97$ kN. In the simulation, the maximum tension immediately following the release of a new point mass spikes to a very large level; since this is an artifact of the discretization of the tether mass, Figure 10d is generated by measuring the tension only directly prior to the release of a new point mass. According to the figure, the maximum tension is never exceeded; it is prudent, however to treat this result with some caution, due to the artifacts resulting from the mass discretization. It should also be noted that this result is sensitive to the tether damping parameter; for example, with the damping reduced by a factor 10, the maximum tension spikes significantly above the maximum limit.

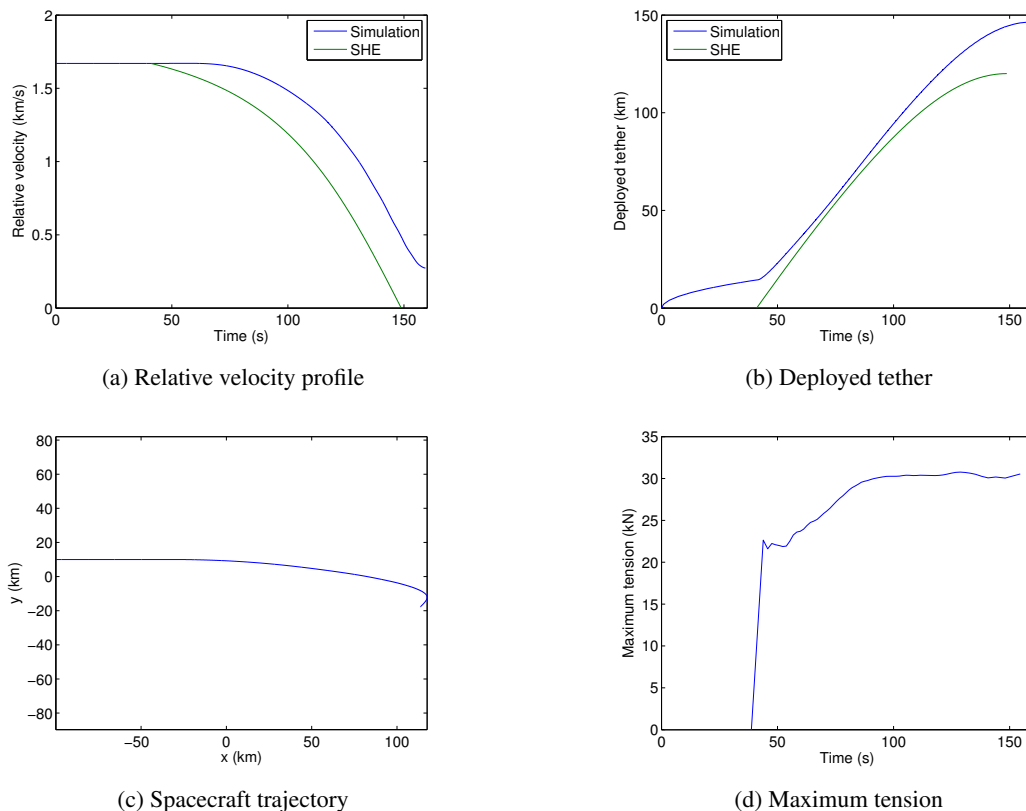
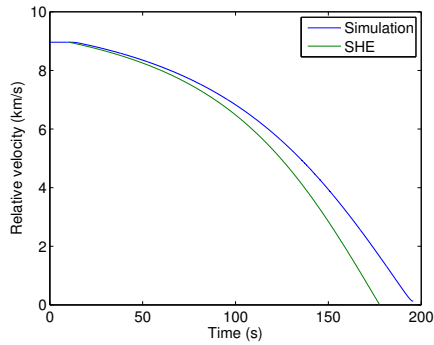
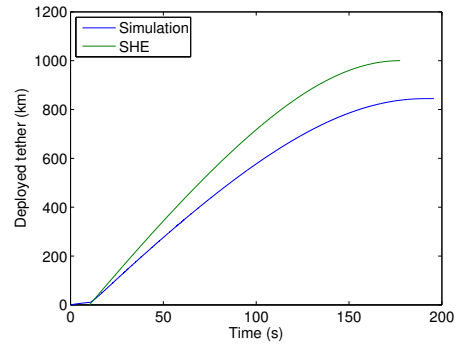


Figure 10: The figures show the results from a simulation using a Zylon tether, and compares these to the results predicted by the assumptions made in the derivation of SHE. Owing to the 2D penalty, more than the available tether is needed; hence, one would need to aim for a lower ΔV in this case.

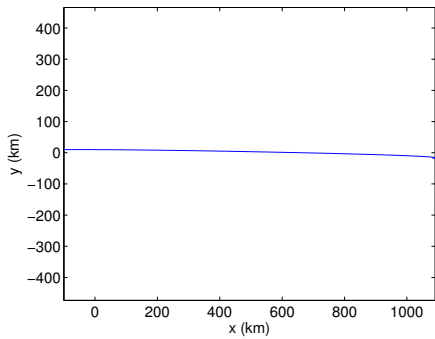
Results from the CNT case can be seen in Figure 11. In this case, the 2D penalty is small relative to the total tether length. Due to the benefits of tether extensibility, less tether is consumed in this case than what is predicted by SHE. The trajectory exhibits only a shallow curvature, as seen in Figure 11c. Figure 11d shows the maximum tension along the line, which never exceeds the limit of $T_{\max} = 107.1$ kN. The maximum tension is measured in the same way as for the Zylon case and is subject to the same caveats.



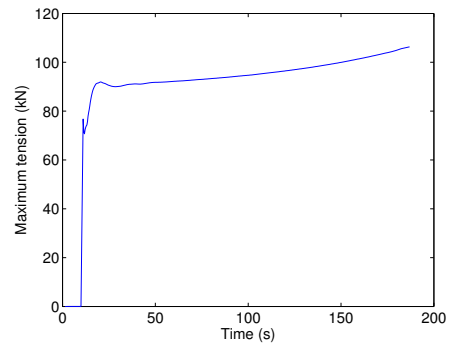
(a) Relative velocity profile



(b) Deployed tether



(c) Spacecraft trajectory



(d) Maximum tension

Figure 11: The figures show the results from a simulation using a CNT tether, and compares these to the results predicted by the assumptions made in the derivation of SHE. Owing to the benefit of tether extensibility and the limited 2D penalty, less tether is needed than what is predicted by SHE.

IV. Harpoon Impact

Harpoon survivability to hypervelocity impact on the target celestial body is critical to the feasibility analysis of the hitchhiker concept. Under certain conditions of impact velocity and material parameters, the distribution of stresses in solid media (both projectile and target) can exceed a threshold value, commonly denominated yield stress. This quantity can be dependent on temperature, loading condition, and rate of loading and determines the inception of a new regime of motion within the material. This new regime is dependent on the crystalline structure of the materials in such a way that some materials, denominated brittle, will fail and fracture, while others, the ductile materials, will undergo irreversible plastic deformations that stay in the solid even when the stresses are removed. Experimental evidence suggests that this plastic state is independent of the hydrostatic stress condition in the solid, enabling a “fluid-like” motion of the solid. The portion of the projectile that undergoes solid deformations loses its strength and can be considered “eroded” from the projectile in a simplified approach. A significant portion of the harpoon is required to remain uneroded (i.e., without plastic deformations) after impact in order to anchor the tether and spacecraft and support the loads developing in the maneuvers required for equalizing the velocities of the spacecraft and target body without detaching. In order to determine what kind of materials can potentially withstand the impact conditions, a 0-D hydrostatic model^{17,18} was first used. This analytical model determines the fraction of the projectile (considered as a long rod) that remains uneroded after the impact as a function of the impact velocity and material properties and, owing to its simplicity, is extremely useful for parametric studies. In order to answer more questions about the feasibility of the mission, a 2-D numerical code, previously developed as a part of a PhD thesis,¹⁴ was employed. This model allowed us to gain insight into the effect of projectile thickness and obliqueness of the impact, and the crater diameters resulting for different impact conditions. The 2-D model was also employed in verification of the 0-D results.

A. 0-D hydrostatic model for hypervelocity impact

1. Derivation of the 0-D model

Our analysis is based on the model developed by Tate.^{17,18} We consider a situation where a projectile of density ρ_p , whose original length is L , penetrates into a semi-infinite target of density ρ_t with initial velocity V_0 , as in Figure 12. We assume that the projectile acts as rigid body until a certain pressure, Y_p , is reached, which is approximated by the Hugoniot Elastic Limit (HEL) of the material. The Hugoniot Elastic Limit is defined as the minimum stress required behind a shock in order to produce permanent deformations in a material. Its relation with the classical static yield stress of the material (i.e., the minimum stress that produces plastic deformations in a classical tension test) depends on the material, with the HEL being typically a few times higher than the static yield stress. In Figure 12, the front part (A-B) of the projectile behaves hydrostatically (i.e., the stress condition can be assimilated to a hydrostatic pressure situation) while the rear part (B-C) remains solid and is modeled as a rigid body. Likewise, the target material behaves as a rigid body below the threshold pressure, R_t . The interface of two materials (A) proceeds through the target material at velocity U , which is slower than V . Taking moving axes across the interface, the two materials can be modeled as colliding flows of incompressible liquid.

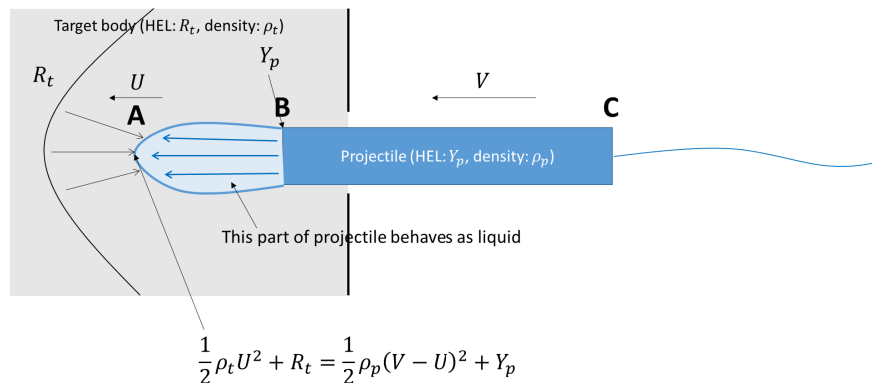


Figure 12: Hydrodynamic model of hypervelocity impact.

In,¹⁷ Bernoulli's equation in the region undergoing plastic deformations and rigid body motion equations for the elastic region of the projectile were used to show that the erosion of the projectile ends once the velocity of the

interface, U , becomes equal to the velocity of the rigid body, V , whenever the strength of the projectile Y_p is higher than the strength of the target R_t (the only case considered here as otherwise the projectile is completely eroded). The velocity at which erosion stops is given in¹⁷ by:

$$V_c = \sqrt{2(Y_p - R_t)/\rho_t}, \quad (19)$$

If the initial velocity, V_0 , of projectile is less than this critical velocity, V_c , then the entire projectile remains in elastic state after the impact. An analytical expression for the remaining length of projectile, l_s , was also given in:¹⁷

$$\frac{l_s}{L} = \left[\sqrt{\frac{\frac{A(\mu+1)}{\mu-1}}{V_0 + \sqrt{V_0^2 + A}}} \right]^{\left(\frac{R_t - Y_p}{\mu Y_p}\right)} \exp \left[\frac{\mu \rho_p}{2(1 - \mu^2) Y_p} \cdot \left\{ V_0 \sqrt{V_0^2 + A} - \mu V_0^2 \right\} \right], \quad (20)$$

where $\mu = \sqrt{\rho_t/\rho_p}$, $A = 2 \frac{(R_t - Y_p)(1 - \mu^2)}{\rho_t}$. If $l_s > 0$, the motion after the point in which further plastic deformations disappear can be assimilated to a rigid body of length l_s being slowed down from the velocity V_c to a stop by the interfacial pressure. The total depth of impact can also be recovered from the analysis since an analytical expression for the interfacial velocity U as a function of time is available. The time integration of U for the duration of the impact motion readily produces the depth d_f .

In Fig. 13, we use the analytical solution above (20) to evaluate the remaining length of projectile at a given velocity and for different candidate projectiles. Hard rock and soft soil targets are considered. The elastic limit and density of the target and projectile materials are given in the legend. The first conclusion that can be extracted from the parametric analysis is that, although the compressive strength of very soft soil and very strong rock are $\sim 10,000$ times different, there is no order-of-magnitude difference in the uneroded length. This phenomenon is due to the strength of the projectile being dominant over the strength of the target in both cases. Indeed, differences observed between the results for soft solid and hard rock are mostly related to the density of the target. Metal materials (steel and tungsten) are completely eroded at 10 km/s impact speed. On the other hand, by using boron carbide and Y2O3-doped zirconia, 16%-27% and 30%-52% of the projectiles remains uneroded, respectively, which would be sufficient to work as a harpoon. Finally, we can set a best case scenario using the strongest known material, diamond. According to Figure 13, 83%-92% of the strongest (and possibly the most expensive projectile in the world) will survive after a 10 km/s impact. With respect to impact depth (not shown in the figure) denser materials, such as tungsten, behave better as their increased inertia results in longer times being required for completely stopping the motion. This result holds as long as they withstand the impact without significant erosion. Thus, a tungsten projectile would be the best candidate at lower velocities, while zirconia may perform better in the range of 3-7 km/s. and diamond at 10 km/s.

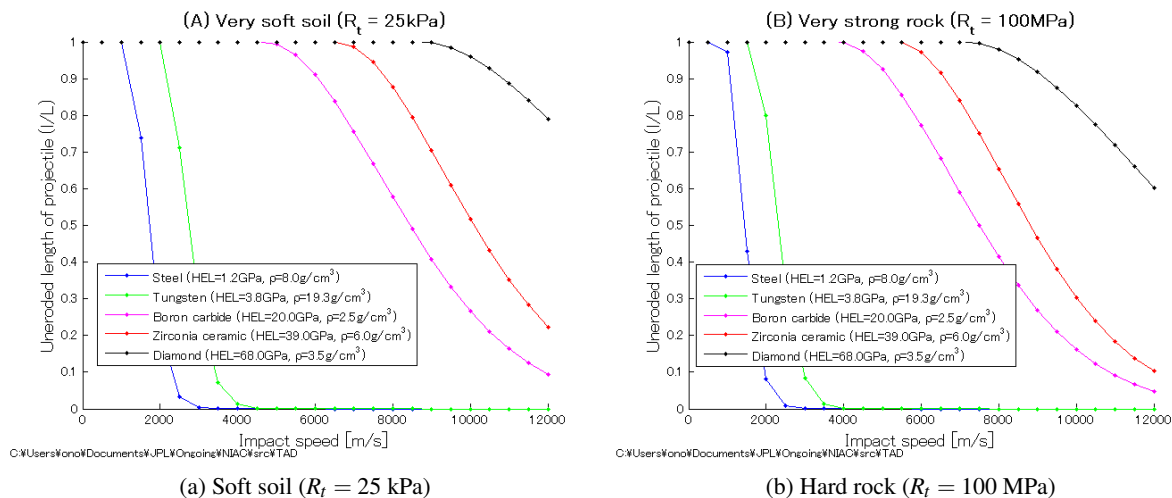


Figure 13: Uneroded length of projectile (l) in relative to the original length (L) after an impact with very soft soil (A) and very strong rock (B). Results are obtained using the 0-D model.

B. Numerical Simulations

2-D numerical simulations of hypervelocity impact of rod projectiles were performed using the Adaptive Mesh Refinement Objected-oriented C++ (AMROC) algorithm. This computer code, which has been used at Caltech for over a decade in the simulation of compressible and turbulent fluid flow, has been extended in the last five years with the implementation of multi-material solid mechanics capabilities specifically suited for the study of metal-metal ductile impacts at high velocities.^{2,14} The approach followed in this algorithm makes use of a CFD-like fixed Eulerian grid for discretizing the computational domain, avoiding the difficulties presented, due to mesh entanglement, in classical computational methods when used to solve for large deformations in solid materials. Simulations were run using the Zodiac cluster at JPL. A typical simulation takes 12 to 24 hours to complete when using 48 computational cores, distributed in 4 nodes. The cell size was chosen to be 0.16% of the initial length of the projectile. The use of 2-D simulations enables the analysis of crater depth and effect of the incidence angle and aspect ratio of the projectile. For perpendicular impacts, cylindrical symmetry along the projectile centerline can be prescribed in a way such that 3-D simulations are not required. For oblique impacts, since a cylindrical axis of symmetry does not exist, we run simplified cases in which the target and projectile are considered infinite in the third dimension. A fully consistent simulation would require the use of three-dimensional computational domains. Due to the high computational cost (even at low resolutions) of 3-D simulations, we decided to run the simplified cases, from where qualitative conclusions can be extracted. 3-D simulations are to be considered for future, more detailed, studies.

A full parametric study, such as the one performed for assessing the length of uneroded projectile with the 0-D model (Figure 13), was not possible due to limitations in the computational resources and the time available to complete this task. Instead, we chose to simulate a subset of cases that provide useful insight into key parameters: material properties and strength of the projectile and target, velocity of impact, angle of incidence, and aspect ratio of the projectile. We considered tungsten, zirconia, and diamond as possible candidates for the rod projectile, and hard rock and soft soil for the target. Due to the higher complexity of the material models used in the 2-D code, new material properties, summarized in Table 2, were considered according to the available literature for each test material. The 2-D code was first used to compare the results of the previous section for tungsten, zirconia, and diamond at 1.5km/s (elastic impact) and 10 km/s (plastic impact). Even when small differences arose between the two models, the conclusions of the 0-D model analysis did not change with the new results. As an example of the differences between the two models, it was found that the deceleration rate of the projectile is higher in the 2-D simulations, resulting in slightly lower penetration depths. This feature can be attributed to a better representation in the 2-D code of shock structures in the target material, which follow a circumferential pattern from the point of impact, and to two-dimensional features arising at the contact interface between materials.

Table 2: Mechanical properties for the materials evaluated with the 0-D, 1-D, and 2-D models

	Projectile			Target	
	Tungsten	Zirconia	Diamond	Hard rock	Soft soil
Density (g/cm ³)	19.25	6.05	3.5	2.7	1.8
Bulk modulus (GPa)	310	170	443	31.7	0.066
Shear modulus (GPa)	161	78.84	478	23.85	0.03076
Heat capacity (J/kg/K)	134	280	516	795	835
Elastic limit (GPa)	3.8	39	68	0.1	0.00025

1. Crater size in perpendicular impact

Results of 2-D simulations at impact velocities of 1.5 km/s, 5 km/s, 8 km/s, and 10km/s are shown for tungsten, zirconia, and diamond projectiles with an aspect ratio L/D of 10. It is expected for the crater diameter to depend on the aspect ratio (an effect not captured by in the 0-D model) and additional simulations were run with lower aspect ratios to assess the importance of this parameter. Those simulations are not shown here for simplicity but reveal that the ratio between the projectile and crater diameter at low impact velocities remains constant while it increases at large velocities. The target material is always hard rock. For each simulation, we show results for depth of impact d_f , crater diameter, and remaining length l_s of the projectile. In order to provide a description as accurate as possible for the crater diameter, we report four different values. d_1 is the diameter at 1/4 of the projectile length from the leading tip, d_2 is the maximum diameter along the axial location of the projectile, d_3 is the maximum diameter in

the radial locations above the projectile within one length of the trailing tip of the projectile, and d_4 is the absolute maximum diameter. Figure 14 shows graphically these diameter definitions. The smaller the ratio between the crater and projectile diameter is at each of this location, the more likely the projectile can become attached to the target material.

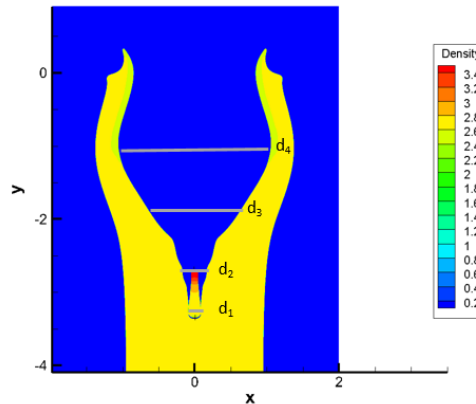


Figure 14: Definition of crater diameters used in Table 6.

The combined analysis of the results in Tables 3-5 reveals that, similarly to what was found in the 0-D model, tungsten is the most appropriate material to be used in low velocity impacts. Due to its larger density, which translates into a higher initial kinetic energy in the system. A tungsten projectile is capable of producing a deeper impact with low crater diameters as long as the material remains in the elastic regime. However, as the velocity of the impact is increased, the option of using a tungsten impactor becomes less optimal. At 5 km/s, only a tiny fraction of the projectile is capable of surviving the impact. At the velocities of 5km/s, zirconia and diamond are the likely choices as these materials do not undergo plastic deformations in this conditions. It can be observed that the penetration depth is maximum (as the kinetic energy of the impact is not lost in plastic deformations of the projectiles) and crater diameters are conducive to the projectile becoming embedded into the target. As the velocity is increased to 8km/s, the impact depth is reduced due to the presence of plastic deformations. This is also translated into larger crater diameters than before. At the same time, radial deformations in the projectiles increase. For this reason, we present the diameter non-dimensionalized with the maximum diameter of the deformed projectile. Results show that there exists some compensation between larger crater diameters and radial deformations of the projectile, and the likelihood of a zirconia or diamond remaining attached to the target is large. In the final case of a 10km/s impact, the only suitable option is diamond. Even when approximately 1/3 of the zirconia projectile survives, the created crater is too wide for any attachment to occur. Even in the case of the diamond projectile, attachment can be compromised in this case.

Finally, Table 6 presents a comparison of crater diameter between a hard rock and soft soil target material. Results suggest that at the low velocity condition, the crater diameter mostly depends on the target material, as the diameters for multiple projectile materials are very similar. It is only in d_3 where significant changes are observed. This is because this value depends on the impact depth. For a deeper impact, such as with tungsten, the crater has a funnel shape while in the case of diamond, its shape is more conical. With respect to the target material, the soft soil deforms more under impact than the hard rock, resulting in larger crater diameters. In Figure 15, we complete this discussion showing the crater and projectile shapes for multiple cases.

2. Oblique impacts

The aim of this subsection is to determine whether the incidence angle of the projectile is a key parameter for this proof of concept. Three additional simulations were run with a carbon projectile and a hard rock target. At 10 km/s, incidence angles of 1 and 10 degrees were tested, while at 1.5 km/s, only the 10 degree case was attempted. For simplicity, these simulations were run in a two-dimensional computational domain, assuming that the materials are infinitely long in the third dimension, while the perpendicular impact cases were run in the same 2-D computational domain including terms that account for cylindrical symmetry around the axial centerline of the projectile. The width of the target was increased to account for the oblique motion of the projectile inside the target.

Figure 16 shows a comparison of the final state of the system for a 1.5km/s impact. The first feature observed as

Table 3: Penetration depth with respect to initial length of projectile, d_f/L (* denotes projectile was still in motion at the end of the simulation)

Material	Impact velocity (km/s)			
	1.5	5	8	10
C+HR	2.38	7.22	4.43	3.36
ZrO2+HR	5.92	8.79*	4.11	3.38
W+HR	8.799*	4.84	2.87	2.93

Table 4: Crater diameter at locations 1, 2, and 3 (see Fig. 14) with respect to deformed maximum diameter of the projectile, D

Material	Impact velocity (km/s)											
	1.5			5.0			8.0			10.0		
	d_1/D	d_2/D	d_3/D	d_1/D	d_2/D	d_3/D	d_1/D	d_2/D	d_3/D	d_1/D	d_2/D	d_3/D
C+HR	1	1.33	1.56	1	1	1.64	1	1.56	3.83	1.00	1.57	3.58
ZrO2+HR	1	1.22	1.24	1	1	1.5	1	1.15	1.68	1.54	2.74	4.27
W+HR	1	1.2	1.5	1	1	1.24	N/A	N/A	N/A	N/A	N/A	N/A

Table 5: Remaining length of projectile with respect to initial length, l_s/L

Material	Impact velocity (km/s)			
	1.5	5	8	10
C+HR	1	1	0.87	0.70
ZrO2+HR	1	0.97	0.50	0.27
W+HR	1	0.1	0	0

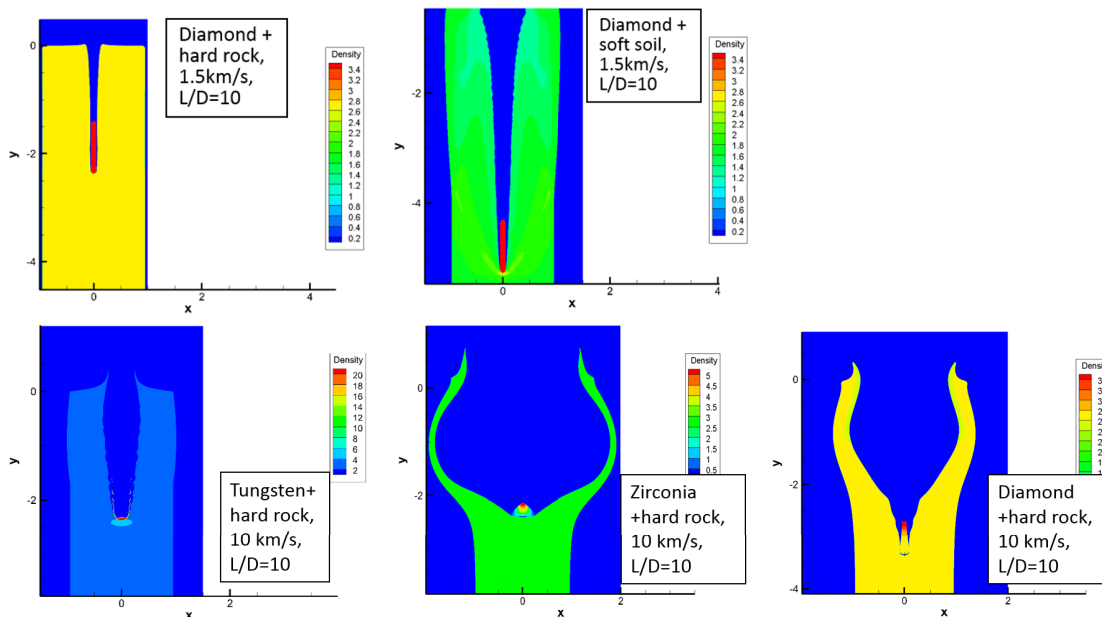


Figure 15: Crater and projectile shapes at the final configuration as a function of target material, impact velocity, and aspect ratio of the projectile.

Table 6: Crater diameters (definitions according to Figure 14) with respect to maximum deformed diameter of projectile D' for projectiles (C=diamond, Zr=zirconia, W=tungsten), targets (HR= hard rock, SS =soft soil), impact velocities and aspect ratios, L/D .

	C+HR, 1.5km/s	C+SS, 1.5km/s	C+HR, 10km/s	C+SS, 10km/s	Zr+HR, 1.5km/s	Zr+SS, 1.5km/s	W+HR, 1.5km/s	W+SS, 1.5km/s
d_1/D'	1	1.56	1	1.41	1	1.54	1	1.70
d_2/D'	1.33	2.15	1.57	2.00	1.22	2.14	1.2	2.2
d_3/D'	1.56	8.21	3.58	2.35	1.24	4.5	1.5	2.5
d_4/D'	3.33	12.3	12.41	13.1	3.26	12.28	3.4	9.62

a result of the oblique impact simulation is that the projectile has reversed its orientation. This phenomenon can be attributed to the angular momentum that is exerted after the initial contact between the projectile and the target. At first instance, the angular momentum tries to expel the projectile (which may happen at higher incidence angles) but as soon as a crater is formed and penetration begins, the projectile is deflected in the opposite direction by the pressure exerted in the radial direction by the target. This phenomenon is exacerbated by the slender shape of the projectile, which produces a long arm for the moments computed around the center of mass of the projectile. It is also noticeable that the crater is much wider and the projectile is not as well embedded as it is in the normal impact case. The ability of the impactor to work as a harpoon is therefore compromised by small deviations in the incidence angle.

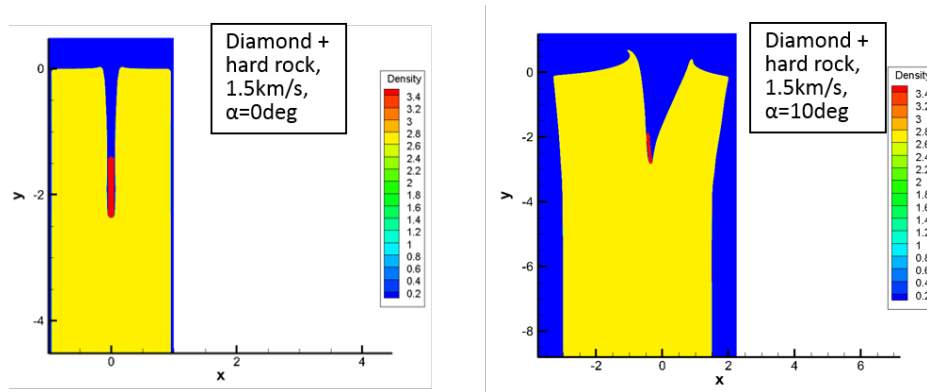


Figure 16: Comparison of crater diameter and final position of the projectile for normal and oblique impacts at 1.5 km/s.

In Figure 17, we present the same comparison for the 10km/s impact, including the case with incidence angle of 1 degree. For this initial condition, the effect of even a very small deviation in the incidence of the projectile is devastating. As in the previous case, the projectile changes its orientation, producing a larger crater. In addition, the projectile is not embedded in the target material. This analysis suggests that the probability of the harpoon attaching to the target in the case of oblique impact at high velocities is extremely remote.

C. Summary of Analysis

A hydrodynamic 0-D analytical model and a 2-D computer code were used in order to assess key questions about the behavior of a rod projectile under hypervelocity impact conditions in rock and soil. The key findings are:

1. At low velocity conditions (1.5km/s), the metal and ceramic materials tested do not undergo plastic deformations and the projectile is intact when it stops inside the material. Crater depths are a typically few times the length of the projectile and increase with the mass of the impactor. In this condition, the tungsten projectile would represent the best option due to its higher density. The crater diameters at low velocities are small, which increases the probability of the harpoon attaching to the geological material of the celestial body. Crater diameters decrease with the strength of the target material so attaching to a strong rock is easier than into soil.
2. At intermediate velocity conditions (5km/s and 8 km/s), tungsten is no longer an option and ceramic materials

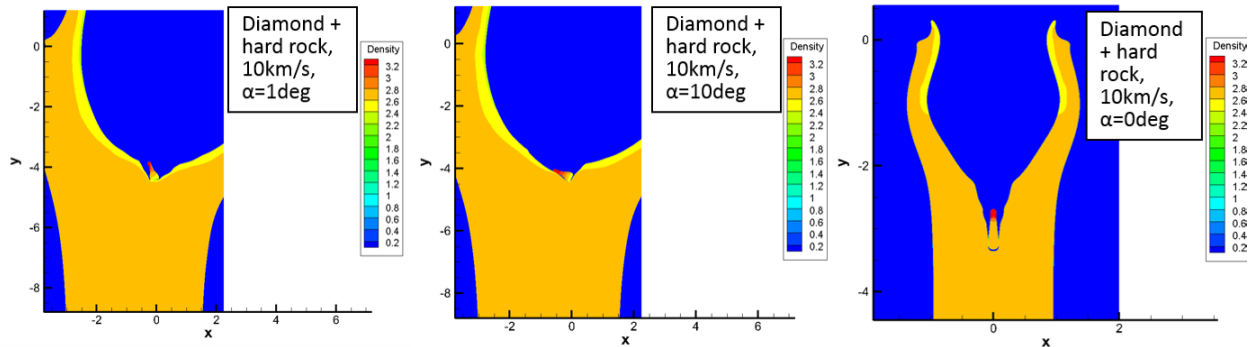


Figure 17: Comparison of crater diameter and final position of the projectile for normal and oblique impacts at 10 km/s.

are required. As the velocity increases, diamond becomes progressively better suited for this application than zirconia.

3. At high velocity conditions (10km/s), only the strongest material tested (diamond) can effectively function as a harpoon. The crater diameters are higher as more initial kinetic energy of the projectile is spent in plastic deformations in both target and projectile. This is also translated into penetration depths not significantly larger than in the 1.5km/s. Even when part of zirconia projectile survives the impact, this material undergoes large radial deformations increasing the diameter of the crater and reducing the depth of impact. A tungsten projectile would be completely destroyed in these conditions.
4. The obliquity of the impact has a profound effect in the crater width and poses a challenge for the Comet Hitchhiker concept. This is due to the shape of the projectile, conducive to large torques produced by the pressure exerted by the target not being aligned to the projectile axis. Simulations show that the projectile can even change orientation during the impact, reducing the probability of becoming embedded in the target material.

Future work in the modeling and simulation front has to be focused in understanding whether certain projectile shapes (like arrowhead or blunt) can minimize the negative effects observed in oblique impacts. Full 3-D simulations appear to be necessary to address this concern as the simplifications used in these simulations (2-D with projectile and target infinitely long in the third dimension) may have contributed to the adverse effects that have been described.

Another factor for uncertainty in these simulations is the approximate values used in the simulations of the target material and ductile plasticity model not being the best model to describe the behavior of soils and rock. If the release of the kinetic energy of the projectile is done through fracture of the material instead of plastic deformations, variables such as crater width may be affected. Combining fracture mechanics with dynamic behavior of materials is not straightforward and may require an effort beyond the scope of this work.

V. Tether Braking

As discussed in Section II, the space hitchhiker maneuver requires braking on tether in order to control tension and accelerate/decelerate the spacecraft. However, due to the very high speed of tether (1-10km/s), conventional brake mechanisms would not likely work. In addition, in order to perform the inverse hitchhike maneuver, a hitchhiker must have a capability to accelerate the tether. Therefore, availability of tether braking/acceleration mechanism that can support the speed required to perform hitchhike maneuvers is a key to the feasibility of the Comet Hitchhiker concept.

In this section, we first investigate contactless linear brake/motor mechanisms that can be potentially used for hitchhikers. Then we perform preliminary feasibility analysis in terms of heat dissipation.

A. Contactless Brake/Motor Mechanisms

Among various brake/motor mechanisms, linear electromagnetic brakes are the most prospective because it does not require physical contact with tether. There are few variants, which are similar but different in energy dissipation

methods.

1. Linear induction brake/motor

Linear induction motor is an alternating current, asynchronous linear motor, which is widely used in train systems such as John F. Kennedy Airport's AirTrain and Tokyo's Toei Oedo subway line. The motor can also be used as a regenerative brake. In the train application, the secondary is a sheet of metal placed between two rails, in which eddy current is induced.

As shown in Figure 18, in the application for hitchhikers, the motor's secondary is the tether itself that goes through a series of coils. The tether must be conductive. We can use either a conductive material, such as carbon nanotube, or conductive textile, such as Zylon fibers plated with metal.

When used as a brake, the induced eddy current produces magnetic field that counteracts the tether motion, as in Figure 18-(a). The eddy current also produces heat in tether due to the resistance. As a result, the kinetic energy of the spacecraft is turned to heat and electric energy, which can be stored in the spacecraft to be used for the next inverse hitchhike maneuver. When used as a motor, the magnetic field produced by the eddy current accelerates the tether by consuming the stored electric energy.

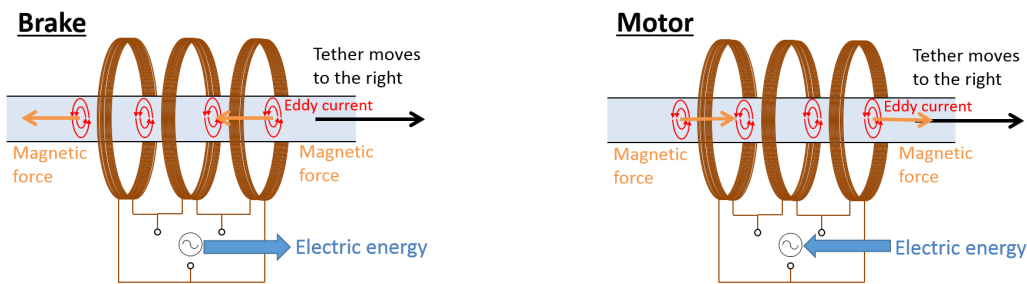


Figure 18: Linear induction brake/motor for Comet Hitchhiker used as (a) brake and (b) motor.

2. Linear eddy current brake

Linear eddy current brake is similar to linear induction motor/brake but has a simpler mechanism, as shown in Figure 19a. A conductive tether goes through DC coils. The coils can be replaced with donut-shaped permanent magnets, but in such a case tether tension cannot be actively controlled. The magnetic field produced by the DC coils induces eddy current in the tether, which counteracts with the DC magnetic field. No electricity is produced in this brake mechanism, hence all the kinetic energy is eventually dissipated as heat in the tether. Importantly, this mechanism cannot be used as a motor. Hence, it cannot be used for a multi-hitchhike mission which requires inverse hitchhike maneuvers. Its major advantage is the simplicity.

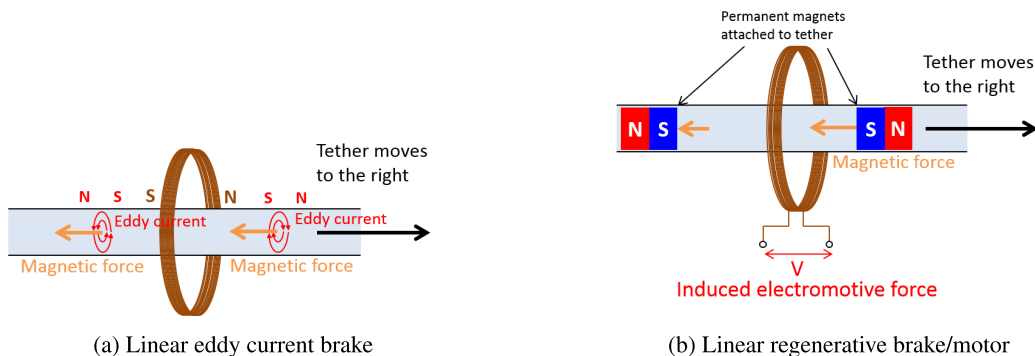


Figure 19: Linear eddy current brake and regenerative brake/motor mechanisms for Hitchhiker

3. Linear regenerative brake/motor

A slightly more complex mechanism is the linear regenerative brake/motor shown in Figure 19b. Non-conducting tether with permanent magnets goes through coils, in which induced electromotive force is produced. An advantage of this mechanism is that no heat is produced in the tether. Furthermore, the same mechanism can be used as a linear motor by injecting electric energy to the coil. A concern is the increase mass of the tether due to the permanent magnets.

B. Heat Dissipation

Heat dissipation is a major technical challenge. We performed preliminary analysis on the temperature increase of tether with following assumptions:

- **Assumption 1:** all the kinetic energy of spacecraft is dissipated as heat only in the tether.
- **Assumption 2:** heat is distributed uniformly through the tether

Assumption 1 is conservative in two aspects. First, in reality, not all the heat goes to the tether; heat in the spacecraft can be dissipated efficiently by radiators, for example. Second, using regenerative brake will significantly reduce the amount of heat produced by braking. On the other hand, Assumption 2 is pessimistic because heat distribution cannot be perfectly uniform. However, this assumption gives a good approximation for materials with a high thermal conductivity such as carbon nanotube.

Let ΔT be the temperature increase of tether, c be the specific heat capacity of tether, m is the mass of the tether, M is the mass of the spacecraft including the tether, and ΔV be the velocity change of the spacecraft. With the above assumptions, ΔT is obtained from the following equation:

$$cm\Delta T = \frac{1}{2}M\Delta V^2.$$

We assume that the mass ratio is 5 i.e., $(M - m)/M = 5$. The specific heat capacity is 5.4 KJ/kgK for CNT⁴ and 1.5 KJ/kgK for Zylon.¹⁹

Table 7: Temperature increase of tether due to braking, with assumption that 1) all the kinetic energy of spacecraft is dissipated as heat only in the tether and 2) heat is distributed uniformly. Using regenerative brake will significantly relax the temperature increase.

ΔV [km/s]	Temperature increase [K]	
	CNT	Zylon
1.0	120	420
2.0	470	1700
4.0	1900	6700

Table 7 summarizes the results. Note that the sublimation temperature is 2900K for CNT²¹ and 600K for Zylon.¹⁹ The result suggests that no active heat dissipation is necessary for both materials for a 1 km/s hitchhike, though the initial temperature of Zylon must be relatively low (≤ 150 K), hence it should be thermally isolated from the heat produced by spacecraft bus before deployment. A CNT tether can withstand up to 4 km/s without active heat dissipation. We note that the strength of material often reduces at a high temperature and we do not consider that effect in this analysis.

In order to perform hitchhike above these limits, regenerative braking, active heat dissipation, or both are required. In particular regenerative brake is beneficial because it can reduce the total amount of heat produced and generate electric energy. The electric energy can be stored in a superconducting coil, for example, to be used for the next inverse hitchhike maneuver. Alternatively, it can be used instantly to drive high-power ion thrusters to provide additional acceleration and hence relax tension on tether.

VI. Mission Analysis

A. Summary of Analysis

There would be two types of hitchhiking missions: *single hitchhike mission (SHM)* and *multi hitchhike mission (MHM)*. SHM is comparable to *Galileo* and *Cassini* missions, where a spacecraft performs a single hitchhike maneuver to rendezvous with a target and observe it for a relatively long duration. MHM is comparable to *Dawn*, where a spacecraft rendezvouses with multiple targets by repeating hitchhike and inverse hitchhike maneuvers. We performed mission utility analysis for both SHM and MHM.

1. Single Hitchhike Mission

Our major findings include followings:

- Orbit insertion ΔV is negatively correlated to the flight time from Earth to the target (See, for example, Figure 20.)
- The minimum ΔV requirement for orbit insertion around small bodies in the outer Solar System (KBOs, Centaurs, Jupiter Trojans) is ~ 1 -2 km/s. This is not impossible but is an unprecedented level of deep space maneuver for chemical propulsion.
- A hitchhiker can provide ΔV that is well beyond the minimum requirement. It is an enabler of the rendezvous missions to small bodies in the outer Solar System. Future advancement in tether materials will further increase available ΔV , which in turn shortens flight time.
- Jupiter flyby is useful to reduce the orbit insertion ΔV by increasing perihelion, but with a cost of a longer flight time. (Intuitively, in this case, we reduce the orbital velocity through fly-by instead of increasing it.)

We performed analysis for four types of targets: KBOs, Centaurs, Jupiter Trojans, and Damocloids. The analysis results are summarized in Table 8. The details of analysis for Pluto rendezvous is presented in Sections VI-B. Note that, for each target, the table shows two extreme design points of a mission (one with the minimum flight time with a 10 km/s upper bound on ΔV , while the other being the minimum ΔV and a long flight time.) The point is that there is a trade-off between ΔV and flight time. A hitchhiker mission can be flexibly designed between the two extrema.

Table 8: Summary of the single hitchhike mission analyses. Shown in the table are two extreme point designs of each mission. The results in the “Min. flight time” columns are obtained by minimizing the flight time with a 10 km/s upper bound on the orbit insertion delta-V. The results in the “Min. ΔV_{OI} ” columns are obtained by minimizing the orbit insertion delta-V.

Mission Concept	Target	Min. flight time s.t. $\Delta V_{OI} \leq 10$ km/s		Min. ΔV_{OI}	
		ΔV_{OI}	Flight time	ΔV_{OI}	Flight time
KBO rendezvous	Pluto (direct)*	10 km/s	13.5 yrs	2.6 km/s	40 yrs
	Pluto (Jupiter fly-by)	10 km/s	16 yrs	1.7 km/s	60 yrs
	Makemake	10 km/s	21.5 yrs	-	-
Centaurs rendezvous	2060 Chiron	7.3 km/s	4.5 yrs	1 km/s	23 yrs
Damocloid rendezvous	1999 RG33	9.6 km/s	1 yrs	-	-
Trojan rendezvous	L4 (659 Nestor)	6.9 km/s	1.9 yrs	2.7 km/s	10 yrs
	L5	-	-	1.5 km/s	16 yrs

*In addition to the orbit insertion maneuver, direct trajectory to Pluto requires a large deep space maneuver (~ 2.1 km) for plane change due to the high orbital inclination of Pluto.

2. Multi Hitchhike Mission

Propellant is gone once it is used. However, a tether can be retrieved after a hitchhiker maneuver for repeated use^d. MHM reinforces the benefit of the Comet Hitchhiker concept as it would enable achievement of greater total ΔV

^dHowever, harpoon is not reusable. Therefore a hitchhiker for MHM would need to carry multiple harpoons.

without increasing significantly increasing spacecraft mass. MHM would also make a hitchhiker useful in a relatively short time since, even with a relatively small ΔV achievable by existing tether materials, a hitchhiker could gain a significant advantage over conventional propulsion for a mission that requires rendezvous with multiple targets.

An ideal near-term destination for MHM would be the main asteroid belt. In fact, as we will discuss in Section VI-C, our study found that rendezvous with multiple targets in the main belt will bring new insights about asteroid families and active asteroids. To demonstrate the feasibility of MHM, we computed a trajectory that sequentially rendezvous with the eight major member of the Themis family. The required ΔV for each hitchhike/inverse hitchhike maneuver is at most 1.6 km/s, which can be achieved by a Kevlar or Zylon tether^e.

In the rest of this section we present detailed analysis results of two specific missions: Pluto rendezvous and MHM to the main belt. The detailed results of other missions in Table 8 are presented in.¹³

B. KBO rendezvous mission

Kuiper belt objects are primordial relics from the protoplanetary disk. Science Objectives would include: 1) Orbit to study the complete surface using optical/IR/gamma ray spectrometry, measure crater counts, dust release through micrometeorite impact, interior structure from orbit perturbations. 2) Use Hitchhiker to circularize the outward trajectory and enable long-term presence in the Belt, e.g. to move from object to object or to measure the micrometeorite and interstellar dust fluxes over a solar cycle.

We performed a detailed trajectory analysis for orbit insertion around Pluto, one of the greatest KBOs. Flight trajectory is optimized with a constraint V_∞ . Figure 20 shows the result of the optimization, where the vertical axis is the flight time while the horizontal axis is V_∞ at arrival.

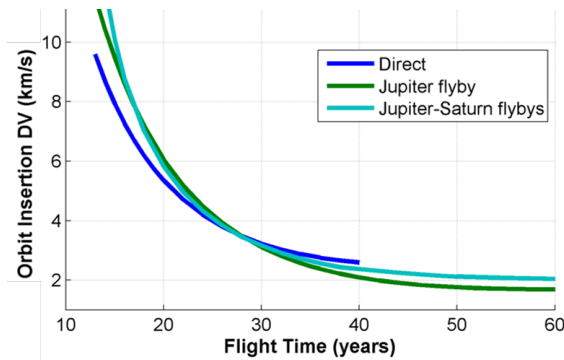


Figure 20: The orbit insertion ΔV to Pluto for trajectories with specified flight time^f. A wide range of trajectory options are available, but a faster flight time can only be achieved with a cost of greater orbit insertion ΔV .

With 10 km/s orbit insertion ΔV , the following two trajectory options are available :

- Direct flight to Pluto (13.5 years). This option is fastest but requires large deep space maneuver (~ 900 m/s) and highest C3 ($\sim 200\text{km}^2/\text{s}^2$). See Figure 20.
- Jupiter flyby (16 years) to slow down the trajectory. This option takes longer flight times but much lower C3 ($\sim 90\text{km}^2/\text{s}^2$) and requires no DSM. Launch opportunities are available in 2015-2017 and 2027-2029.

As shown in Figure 20, the flight time and orbit insertion ΔV is negative correlated. Therefore, if a hitchhiker maneuver greater than 10 km/s is made feasible by future advancement in tether material, the flight time of Pluto Hitchhiker could be shorter. Performing a 10km/s maneuver in deep space by chemical propulsion is practically impossible since, with $\text{ISP} = 312$ sec (same as Cassinis main engine), 96% of the spacecraft mass must be occupied by propellant.

With a longer flight time, the orbit insertion ΔV can be smaller, but there is a lower bound, as shown in 20. We cut off the analysis at 40 years for direct flight and at 60 years for Jupiter flyby and Jupiter-Saturn flyby. The direct flight option has disadvantage in that it requires deep space maneuver, which cannot be performed by hitchhiking. The Jupiter fly-by option with 60 year flight time requires a 1.7 km/s orbit insertion $\Delta - V$.

^eHowever, the orbit insertion maneuver with the first target would require greater ΔV than the feasible range with Kevlar/Zylon. Hence the first rendezvous would require a combination of hitchhike and conventional propulsion.

As we discuss in Section III, 1.7 km/s hitchhike can be performed by existing tether materials, such as Zylon. On the other hand, 10 km/s hitchhike would require a carbon nanotube tether. This poses an interesting trade-off between mission duration and technology development time. The two extreme ways to design a Pluto rendezvous mission are:

1. Use existing technologies to build a hitchhiker that can perform 1.7 km/s maneuver, launch it in near-term, and wait for 60 years until the rendezvous, or
2. Wait until CNT technologies mature, build a hitchhiker that can perform 10 km/s maneuver, and arrive at Pluto within 15 years from launch.

A realistic option should lie between the two extremums. A Pluto hitchhike mission should be designed to balance science return, required technology development, mission cost, and risk.

C. Multi-hitchhike tour in the main belt

ASTEROID FAMILY Asteroid families are dynamically associated groups of asteroids thought to have been produced by hypervelocity impact destruction of parent bodies.¹⁰ Families are identified by backwards integration of the orbits, showing convergence at some time in the past (which defines the time of breakup). Ages of families range from <1Myr to >Gyr. Hitchhiker would enable visits to a number of components of a collisionally disrupted asteroid. The science would lie in using the fragments to piece together the original. For example, in a young family, one could use optical and near IR imaging to map structure and composition of the fragments. One aim would be to distinguish pieces of the core from pieces of the mantle of the precursor, to test models of the asteroid disruption process. Gravitational deflection of each fragment (i.e., before or after tether attachment) would give the mass (for big objects, anyway). Images would give the volume. Together, the density is revealed and the density couples with the composition to further characterize the asteroid fragments and the precursor. Asteroid breakup models are very sophisticated. They deserve stronger confrontation with data than has so far been possible.

ACTIVE ASTEROIDS Several interesting groups of asteroids have been identified based on their physical (as opposed to dynamical) properties. Notably, the Active Asteroids (=Main-Belt Comets) are objects in the main asteroid belt which share the dynamical character of asteroids with the physical appearances of comet.^{6,7} They eject dust like comets, some of them because they unexpectedly contain ice. Science significance is that they are potential or likely sources for terrestrial planet volatiles, including the Earth's oceans. An interesting multi-object mission would be to visit a set of Active Asteroids. Science aim would be to characterize their surfaces and identify the source of activity. Cameras would provide high res mapping in optical and IR. Value of a multi-mission is to study them as a group, instead of one-by-one, as so to more quickly gain a proper view of them. Another, smaller, set of asteroids show spectroscopic evidence for surface ice (Themis and Cybele are best examples, Themis is the archetype of a 2 Gyr old family). Another interesting class of asteroids are ice-coated ones. There are many unanswered questions: Is it really ice? Where is it (poles vs equator vs crater floors etc). What kind of ice is it? Where's it from? In-situ analysis of multiple objects by a hitchhiker will enable to answer these fundamental questions.

TRAJECTORY ANALYSIS The previous mission concepts of Comet Hitchhiker involve a rendezvous with a single object, such as an asteroid. The next logical step of analysis would be to visit multiple main belt asteroids by repeating tether hitchhikes. In fact, a main belt asteroid tour requires extremely high velocity change over the mission lifetime, which would pose major propellant mass challenges for conventional propulsion systems. For instance, the Dawn mission will only visit two main belt asteroids, Vesta and Ceres, despite using highly efficient electric propulsion engines. On the other hand, Comet Hitchhiker is propellant-less, so the limit to mission duration and the number of asteroids studied is only determined by the reliability of the spacecraft and the tether. In particular, particular attention should be given to the amount of micrometeoroids in specific regions of the asteroid belt that could damage or cut the tether.

As described in Section VI-C, a scientifically attractive multi-asteroid tour scenario would be to visit numerous members of a main belt asteroid family. In this report, we consider the Themis family as the reference target because it is one of the major dynamical families of asteroids: it contains more than 500 members with relatively low orbital plane inclinations (which facilitates the transfers between them), and is of significant scientific interest.² Within the Themis family, a subset of 8 asteroids (corresponding to the largest and earliest-discovered members) is selected to generate a tour. This early pruning makes the tour design the more tractable with the limited resources of a NIAC Phase 1 study. In addition, to further simplify the problem, only the inter-asteroid segments of the trajectory are considered. We assume that another propulsion system is used from launch to the first asteroid rendezvous.

Table 9 gives the orbital characteristics of the Themis asteroids selected for the mission. As expected, they have very similar semi-major axes, eccentricities, and inclinations.

Table 9: Themis family members considered for the multi-hitchhike tour

Asteroid	Semi-major axis (AU)	Eccentricity	Inclination (deg)
24 Themis	3.135	0.126	0.752
62 Erato	3.128	0.171	2.230
90 Antiope	3.151	0.165	2.207
104 Klymene	3.149	0.156	2.789
171 Ophelia	3.129	0.132	2.547
468 Lina	3.132	0.198	0.437
526 Jena	3.120	0.135	2.173
846 Lipperta	3.127	0.183	0.264

The mission design goal is to select an asteroid itinerary such that all the asteroids of Table 9 can be visited given ΔV and mission duration constraints. This problem bears similarity to the famous traveling salesman problem (TSP), in which the goal is to find the shortest possible route that visits completely a set of N cities. In the case of our asteroid tour problem, the list of asteroids to visit must be ordered such that the flight time of the mission is minimized. However, finding such a good asteroid itinerary is an extremely challenging combinatorial problem. Exhaustively sampling all possible asteroid ordered sets yields 40320 permutations, which is a large number to sample. This huge search space must also include all the possible time variations within a given sequence.

The solution methodology to generate feasible asteroid itineraries is described herein. The general approach is to consider all asteroid-asteroid segments independently. First, for each asteroid-asteroid pair, a grid of times is formed by varying, at a scan resolution of 30 days, the initial time at the first asteroid between 2035 and 2070 and the flight time between asteroids between 1 and 5 years. The corresponding grid of transfer points is shown in Figure 21.

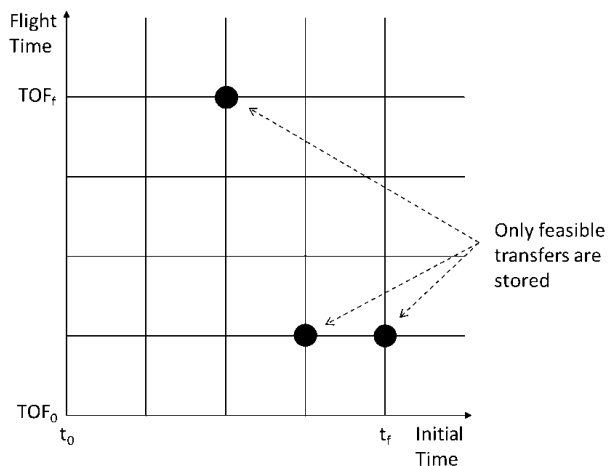


Figure 21: Asteroid-asteroid transfer grid points

Each grid point is associated with a unique combination of initial time and flight time, therefore the grid offers all possible transfer trajectories for a given asteroid-asteroid pair. The impulsive transfers for each point on the grid are computed using a simple Lambert targeting algorithm. The mass of the asteroids are assumed negligible. The Lambert fits provide the incoming and outgoing velocities at the asteroids, which can be converted into DVs from the asteroid velocities. Only feasible transfers are stored based on a given maximum tether ΔV capability, which can result in a dramatic filtering of the search space. To focus on near-term applications, an upper bound ΔV of 1.6 km/s is chosen (within the capability of Kevlar materials).

A tree search is then performed based on the database of acceptable transfers to combine impulsive arcs and form a feasible end-to-end trajectory. To allow enough time for performing science activities, a 55-day minimum stay time

constraint is enforced at each visited asteroid.

This algorithm produced a feasible solution visiting all 8 major members of the Themis, with a total flight time of approximately 34 years and a total required ΔV of 20 km/s. Note that solutions with shorter flight times are expected if flybys of smaller members of the family are exploited, since these extra flybys could also produce significant ΔV maneuvers using the same Comet Hitchhiker technique. Table 10 presents the main characteristics of the feasible multi-hitchhike Themis tour, including departure dates, flight times, stay times, and maneuver magnitudes for each segment of the mission. The corresponding trajectory is shown in Figure 22.

Table 10: Characteristics of the multi-hitchhike Themis tour

Segment	Dep. Date	TOF (years)	Stay time (days)	ΔV_{dep} (km/s)	ΔV_{arr} (km/s)
Ophelia to Klymene	06/03/2036	3.45	456.25	1.56	1.57
Klymene to Erato	02/13/2041	4.40	54.75	1.56	1.60
Erato to Lipperta	08/31/2045	4.90	430.70	0.87	1.60
Lipperta to Lina	09/28/2051	4.95	65.70	1.16	1.60
Lina to Jena	11/13/2056	4.30	87.6	1.48	1.49
Jena to Themis	05/28/2061	2.00	846.80	1.53	1.06
Themis to Antiope	09/21/2065	4.64	N/A	1.53	1.60

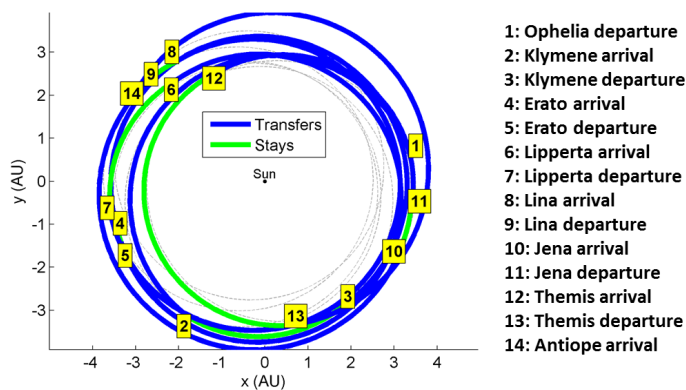


Figure 22: Trajectory and events of the multi-hitchhike Themis tour.

VII. Conclusions

We proposed the Comet Hitchhiker concept, which is to perform momentum exchange with small bodies using an extendable/retrievable tether and a harpoon. The Space Hitchhiker Equation was derived, which gives the achievable ΔV of a Hitchhiker as a function of the specific strength and the mass fraction of tether. The basic feasibility of the concept was assessed through finite element simulations of tether dynamics as well as hypervelocity impact simulations of harpoon. We found that a hitchhike maneuver with $\Delta V \approx 1.5$ km/s is feasible with flight proven materials such as Kevlar/Zylon tether and tungsten harpoon. A carbon nanotube tether, combined with diamond harpoon, would enable ~ 10 km/s hitchhike maneuver. We also presented two particular mission scenarios for Hitchhiker: Pluto rendezvous and a multi-hitchhike mission to the Themis family asteroids in the main belt.

Acknowledgments

The research was carried out in part at the Jet Propulsion Laboratory, California Institute of Technology, under a contract with the National Aeronautics and Space Administration, and in part at University of California, Los Angeles. The authors gratefully acknowledge the NASA Innovative Advanced Concepts program for funding support of this work.

References

- ¹Allison M. Beese, Xiaoding Wei, Sourangsu Sarkar, Rajaprakash Ramachandramoorthy, Michael R. Roenbeck, Alexander Moravsky, Matthew Ford, Fazel Yavari, Denis T. Keane, Raouf O. Loutfy, SonBinh T. Nguyen, and Horacio D. Espinosa. Key factors limiting carbon nanotube yarn strength: Exploring processing-structure-property relationships. *ACS Nano*, 8(11):11454–11466, 2014. PMID: 25353651.
- ²J. C. Castillo-Rogez and B. E. Schmidt. Geophysical evolution of the themis family parent body. *Geophysical Research Letters*, 67(10), 2010.
- ³B.G Demczyk, Y.M Wang, J Cumings, M Hetman, W Han, A Zettl, and R.O Ritchie. Direct mechanical measurement of the tensile strength and elastic modulus of multiwalled carbon nanotubes. *Materials Science and Engineering: A*, 334(12):173 – 178, 2002.
- ⁴Yuan Gao, Amy M Marconnet, Rong Xiang, Shoichi Maruyama, and Kenneth E Goodson. Heat capacity, thermal conductivity, and interface resistance extraction for single-walled carbon nanotube films using frequency-domain thermoreflectance. *Components, Packaging and Manufacturing Technology, IEEE Transactions on*, 3(9):1524–1532, 2013.
- ⁵Tim Hoyer Jack Chan, Dennis Hill and Douglas Leland. Development of advanced stirling radioisotope generator for planetary surface and deep space missions. In *Proceedings of the 6th International Energy Conversion Engineering Conference (IECEC)*, 2008.
- ⁶David Jewitt. The active asteroids. *The Astronomical Journal*, 143, 2012.
- ⁷David Jewitt, Jessica Agarwal, Nuno Peixinho, Harold Weaver, Max Mutchler, Man-To Hui, Jing Li, and Stephen Larson. A new active asteroid 313p/gibbs. *The Astronomical Journal*, 149(2):81, 2015.
- ⁸Eugene M. Levin. *Dynamic Analysis of Space Tether Missions*. Univelt, 2007.
- ⁹Z. Lin. *Low gain feedback*. Springer, 1999.
- ¹⁰Andrea Milani, Alberto Cellino, Zoran Kneevi, Bojan Novakovi, Federica Spoto, and Paolo Paolicchi. Asteroid families classification: Exploiting very large datasets. *Icarus*, 239(0):46 – 73, 2014.
- ¹¹Ajay K. Misra. Overview of nasa program on development of radioisotope power systems with high specific power. In *Proceedings of 4th International Energy Conversion Engineering Conference and Exhibit (IECEC)*, 2006.
- ¹²Steven R. Oleson, Leon Gefert, Michael J. Patterson, Jeffrey Schreiber, Scott Benson, and Jim McAdams. Radioisotope electric propulsion for fast outer planetary orbiters. In *Proceedings of the 38th AIAA/ASME/SAE/ASEE Joint Propulsion Conference and Exhibit*, 2002.
- ¹³Masahiro Ono, Marco Quadrelli, Gregory Lantoine, Paul Backes, Alejandro Lopez Ortega, Håvard Grip, Chen-Wan Yen, and David Jewitt. Comet hitchhiker (niac phase i final report), 2015.
- ¹⁴A. López Ortega, M. Lombardini, D.I. Pullin, and D.I. Meiron. Numerical simulation of elastic-plastic solid mechanics using an eulerina stretch tensor approach and hlld riemann solver. *Journal of Computational Physics*, 257:414–441, 2014.
- ¹⁵J. Park and K. Lee. Carbon nanotube yarns. *Korean Journal of Chemical Engineering*, 2012.
- ¹⁶P. A. Penzo and H. L. Mayer. Tethers and asteroids for artificial gravity assist in the solar system. In *AIAA/AAS Astrodynamics Conference*, 1984.
- ¹⁷A. Tate. A theory for the deceleration of long rods after impact. *Journal of the Mechanics and Physics of Solids*, 15(6):387 – 399, 1967.
- ¹⁸A. Tate. Further results in the theory of long rod penetration. *Journal of the Mechanics and Physics of Solids*, 17(3):141 – 150, 1969.
- ¹⁹Toyobo Co., Ltd. Technical information of pbo fiber zylon, 2001.
- ²⁰Y. Tsuda, O. Mori, R. Funase, H. Sawada, T. Yamamoto, T. Saiki, T. Endo, and J. Kawaguchi. Flight status of {IKAROS} deep space solar sail demonstrator. *Acta Astronautica*, 69(910):833 – 840, 2011.
- ²¹Xianlong Wei, Ming-Sheng Wang, Yoshio Bando, and Dmitri Golberg. Thermal stability of carbon nanotubes probed by anchored tungsten nanoparticles. *Science and Technology of Advanced Materials*, 12(4):044605, 2011.
- ²²Rufan Zhang, Yingying Zhang, Qiang Zhang, Huanhuan Xie, Weizhong Qian, and Fei Wei. Growth of half-meter long carbon nanotubes based on schulzflory distribution. *ACS Nano*, 7(7):6156–6161, 2013. PMID: 23806050.